THE JOURNAL OF BIOLOGICAL CHEMISTRY VOL. 290, NO. 42, pp. 25275–25292, October 16, 2015

Differential Recognition Preferences of the Three Src Homology 3 (SH3) Domains from the Adaptor CD2-associated Protein (CD2AP) and Direct Association with Ras and Rab Interactor 3 (RIN3)*[S]

Received for publication, January 8, 2015, and in revised form, August 17, 2015 Published, JBC Papers in Press, August 20, 2015, DOI 10.1074/jbc.M115.637207

Evgenia Rouka[‡1,2], Philip C. Simister[‡1,3], Melanie Janning[‡1,4], Joerg Kumbrink[§5], Tassos Konstantinou[‡], João R. C. Muniz[¶6], Dhira Joshi[‖], Nicola O'Reilly[‖], Rudolf Volkmer[**], Brigitte Ritter[§], Stefan Knapp[¶], Frank von Delft[¶‡‡§§], Kathrin H. Kirsch[§], and Stephan M. Feller[‡¶¶7]

From the [‡]Weatherall Institute of Molecular Medicine, Department of Oncology, University of Oxford, Oxford OX3 9DS, United Kingdom, the [¶¶]Institute of Molecular Medicine, Martin Luther University Halle-Wittenberg, D-06120 Halle, Germany, the [§]Department of Biochemistry, Boston University School of Medicine, Boston, Massachusetts 02118, the [¶]Structural Genomics Consortium, Nuffield Department of Clinical Medicine, University of Oxford, Oxford OX3 7DQ, United Kingdom, the [‖]Peptide Chemistry Laboratory, London Research Institute Cancer Research UK, London WC2A 3LY, United Kingdom, the [**]Institute of Medical Immunology, Charité-Universitätsmedizin Berlin, 10115 Berlin, Germany, the [‡‡]Diamond Light Source Ltd., Harwell Science and Innovation Campus, Didcot OX11 0QX, United Kingdom, and the [§§]Department of Biochemistry, University of Johannesburg, Auckland Park 2006, South Africa

Background: The CD2AP adaptor facilitates cell signaling using its in-built interaction modules (SH3 domains).
Results: RIN3 was characterized as a novel CD2AP SH3 binding protein by biophysical and biochemical methods.
Conclusion: CD2AP has many potential interactors and is probably a cellular hub.
Significance: We reveal how protein modules can interact with families of related recognition motifs rather than a single motif.

CD2AP is an adaptor protein involved in membrane trafficking, with essential roles in maintaining podocyte function within the kidney glomerulus. CD2AP contains three Src homology 3 (SH3) domains that mediate multiple protein-protein interactions. However, a detailed comparison of the molecular binding preferences of each SH3 remained unexplored, as well as the discovery of novel interactors. Thus, we studied the binding properties of each SH3 domain to the known interactor Casitas B-lineage lymphoma protein (c-CBL), conducted a peptide array screen based on the recognition motif P*x*P*x*PR and identified 40 known or novel candidate binding proteins, such as RIN3, a RAB5-activating guanine nucleotide exchange factor. CD2AP SH3 domains 1 and 2 generally bound with similar characteristics and specificities, whereas the SH3-3 domain bound more weakly to most peptide ligands tested yet recognized an unusually extended sequence in ALG-2-interacting protein X (ALIX). RIN3 peptide scanning arrays revealed two CD2AP binding sites, recognized by all three SH3 domains, but SH3-3 appeared non-functional in precipitation experiments. RIN3 recruited CD2AP to RAB5a-positive early endosomes via these interaction sites. Permutation arrays and isothermal titration calorimetry data showed that the preferred binding motif is P*x*(P/A)*x*PR. Two high-resolution crystal structures (1.65 and 1.11 Å) of CD2AP SH3-1 and SH3-2 solved in complex with RIN3 epitopes 1 and 2, respectively, indicated that another extended motif is relevant in epitope 2. In conclusion, we have discovered novel interaction candidates for CD2AP and characterized subtle yet significant differences in the recognition preferences of its three SH3 domains for c-CBL, ALIX, and RIN3.

CD2-associated protein (CD2AP[8]; or CMS (Cas ligand with multiple Src homology 3 domains) is a multifunctional adaptor protein of 71 kDa, found ubiquitously in the body. First characterized as interacting with the T-cell surface antigen, CD2 (1), and the docking protein p130^{cas} (also known as BCAR1) (2), CD2AP is an essential protein for the proper functioning of the kidney glomerulus, playing a particularly important role in the

* This work was supported, in whole or in part, by National Institutes of Health Grant CA143108 (to K. H. K). The authors declare that they have no conflicts of interest with the contents of this article.
The atomic coordinates and structure factors (codes 4WCI and 3U23) have been deposited in the Protein Data Bank (http://wwpdb.org/).
[S] This article contains supplemental Fig. S1 and Tables S1 and S2.
[1] These authors contributed equally to this work.
[2] Supported by the Medical Research Council, Funds for Women Graduates, and University of Oxford.
[3] Supported by Breast Cancer Now, University of Oxford, and the Rosetrees Trust. To whom correspondence should be addressed: Sir William Dunn School of Pathology, University of Oxford, South Parks Rd., Oxford OX1 3RE, UK. E-mail: philip.simister@imm.ox.ac.uk.
[4] Supported by a DAAD (Deutscher Akademischer Austauschdienst) fellowship. Present address: Dept. of Hematology and Oncology, BMT with Section of Pneumology, and Dept. of Tumor Biology, Hamburg-Eppendorf University Hospital, 20246 Hamburg, Germany.
[5] Supported by Susan G. Komen for the Cure Breast Cancer Foundation Postdoctoral Fellowship KG101208.
[6] Present address: São Carlos Institute of Physics, University of São Paulo, 13566-590 São Carlos, Brazil.
[7] Supported by Breast Cancer Now and EU FP7 Grant Targetbinder. To whom correspondence should be addressed. E-mail: stephan.feller@uk-halle.de.

[8] The abbreviations used are: CD2AP, CD2-associated protein; c-CBL or CBL, Casitas B-lineage lymphoma protein; SH3, Src homology 3; LOAD, late onset Alzheimer disease; CIN85, Cbl-interacting protein of 85 kDa; PRR, proline-rich region; aa, amino acid(s); ITC, isothermal titration calorimetry; Ab, antibody; ZO-1 and ZO-2, zona occludens protein 1 and 2, respectively.

development of the slit diaphragm. Homozygous CD2AP$^{-/-}$ mice develop progressive glomerular malfunction caused by the loss of podocyte foot process integrity and die of renal failure within 6–7 weeks (3). Mutations identified in *CD2AP* (single nucleotide polymorphisms or deletions leading to protein sequence changes) result in abnormal kidney function and proteinuria with nephrotic syndrome caused by focal segmental glomerulosclerosis (4, 5).

Apart from podocytes, CD2AP has been studied in T-cells and dendritic cells among others. CD2AP plays an integral role in actin dynamics, endocytosis of cell surface receptors, and their degradation (*e.g.* binding to F-actin and promoting actin bundling (6); promoting internalization of EGF receptor (7) and VEGF receptor (8); and down-regulation of the T-cell receptor (9), the HER2 (ErbB2) receptor in a subset of breast cancers (10), and the RET (rearranged during transfection) receptor (11, 12)). Conversely, CD2AP positively regulates the plasmacytoid dendritic cell receptor BDCA2; its degradation occurs only with a lack of CD2AP activity (13).

CD2AP can facilitate branched actin filament formation by direct interactions with actin capping protein and cortactin, giving rise to lamellipodia (14). A more direct activity in actin barbed-end capping at adherens junctions was recently reported (15). Various other CD2AP-interacting proteins have been identified, many of which are involved in vesicle trafficking and endocytosis, including the ubiquitin ligases c-CBL (herein termed CBL) (16) and CBL-b (17). Increasingly, endocytosis pathway genes (*e.g. BIN1*/amphiphysin II) are implicated in causal mechanisms underpinning late onset Alzheimer disease (LOAD) (18). Recently, CD2AP was strongly linked to LOAD through genome-wide association studies (19, 20).

CD2AP and its homologue Cbl-interacting protein of 85 kDa (CIN85) are composed of three Src homology 3 (SH3) domains in the N-terminal half followed by a proline-rich region (PRR) and a coiled-coil domain at the C terminus, interspersed with apparently intrinsically disordered regions. CD2AP differs from CIN85 by the presence of additional actin binding sites before the coiled-coil domain (Fig. 1*A*). SH3 domains are globular protein interaction modules, typically binding to proline-rich linear recognition motifs. A large subset of CD2AP interactions involves one or more of its SH3 domains. However, the protein sequences of human CD2AP SH3 domains are only moderately conserved: SH3-2 and SH3-3 share the highest pairwise global sequence identity of only 45%; SH3-1 and SH3-2 have 40% identity; and SH3-1 and SH3-3 have 38% (Fig. 1*B*).

Different biological processes regulated by CD2AP require specific binding partners, illustrating the versatility of CD2AP as an adaptor and hinting that each SH3 may have unique properties and requirements for binding. The key to understanding how specificity and selectivity are achieved to regulate multiple, heterogeneous binding events thus lies in combined knowledge of each molecular interaction. Most *in vitro* studies on the relationships between CD2AP SH3 domains and protein partners have tended to focus on a single domain or partner. None have systematically compared the binding modes of all three SH3 domains in comparative analyses with multiple interactors.

Therefore, we investigated the similarities and differences in the preferences governing protein interactions of each CD2AP SH3 domain with known and novel partners. Based on the P*x*P*x*PR motif, which is characteristic for CBL peptide binding to SH3 domains, we used an *in vitro* peptide array screen to confirm interaction candidates, many with previously uncharacterized sequence requirements. Among 40 binders reported, including ALIX, BLNK, and zona occludens protein 2 (ZO-2), we followed up on the newly identified RIN3, a RAB5 and RAB31 guanine nucleotide exchange factor involved in endocytosis (21, 22), which we identified as a novel interactor in kidney and MCF10A breast cancer cells by several biochemical and biophysical methods.

Experimental Procedures

Generation of Expression Constructs

The sequences encoding the three human CD2AP SH3 domains, herein referred to as SH3-1, SH3-2, and SH3-3, were generated as follows: SH3-2, SH3-3, and SH3-3L (a longer form of SH3-3) were amplified by polymerase chain reaction (PCR) using *Pfu* polymerase; *CD2AP SH3-2*, *-3*, or *-3L* BamHI forward primer; *CD2AP SH3-2*, *-3*, or *-3L* EcoRI reverse primer; and full-length CD2AP cDNA (23) as template before subcloning into BamHI/EcoRI-digested pGEX-6P-1 (SH3-2 and -3) or pGEX-KN (SH3-3L) vectors. Primer sequences were as follows: *CD2AP SH3-2*-BamHI forward, 5′-CG GGATCC AAGAAGCGTCAGTGTAAAGTTC-3′; *CD2AP SH3-2*-EcoRI reverse, 5′-ATA GAATTC CTA TGTTACCTCTAATTCTTTCAC-3′; *CD2AP SH3-3*-BamHI forward, 5′-CG GGATCC GCTAAAGAATATTGTAGAACA-3′; *CD2AP SH3-3*-EcoRI reverse, 5′-ATA GAATTC CTA GTCTTTATCAAGTTC-3′; *CD2AP SH3-3L*-BamHI forward, 5′-ATA GGATCC GGT ACCGAAGGTAAAAT-3′; *CD2AP SH3-3L*-EcoRI reverse, 5′-ATA GAATTC CTA GTCTTTATCAAGTTC-3′. A thrombin site was inserted 5′ of the SH3-3L sequence using the QuikChange^{TM} XL site-directed mutagenesis kit (Agilent Technologies). SH3-1 was synthesized with BamHI and EcoRI restriction sites and cloned into pUC57 by GenScript Corp. The cDNA fragment was subcloned into BamHI/EcoRI-digested pGEX-6P-1 vector. The sequence encoding human RIN3 spanning aa 378–467 encompassing motif-bearing epitopes 1 and 2 (RIN3e1 and -e2) was amplified by PCR using *Pfu* polymerase with RIN3-AA378F-BamHI forward (5′-ATA GGATCC GCG AAG AAG AAC CTT CC-3′) and RIN3-AA467-R-EcoRI reverse primer (5′-ATA GAATTC CTA AGA GAT CCG TTT TTT CCT GG-3′) using full-length Myc-tagged RIN3 cDNA (kindly provided by Dr. T. Katada) (24) as a template and subcloned into BamHI/EcoRI-digested pGEX-6-P-1. Myc- and RFP-tagged RIN3 single and/or double epitope P*xxxx*R → A*xxxx*A mutants were generated using wild-type RIN3 cDNA and the QuikChange^{TM} XL kit. All constructs were validated by DNA sequencing. A Qiagen Plasmid Maxi Kit was used to prepare DNA.

Protein Expression and Purification

GST fusion proteins were expressed in *Escherichia coli* BL21(DE3) and purified essentially as described (25). Eluted GST fusion proteins were dialyzed against the final buffer (5 mM Tris, pH 7.0, 2 mM β-mercaptoethanol), and their integrity was confirmed by SDS-PAGE and Coomassie Blue staining;

protein concentrations were assayed by the Bradford method. Purified proteins were snap-frozen in aliquots and stored at −80 °C until further use in peptide arrays or GST pull-downs.

For isothermal titration calorimetry (ITC) and crystallization, proteins were purified as described above, and the GST tags were cleaved by incubation with PreScission Protease (GE Healthcare) in 20 mM Tris, pH 7.5, 150 mM NaCl. The GST tag and cleaved protein were separated by size exclusion chromatography on a HiLoad 16/60 Superdex 75 column equilibrated with column buffer (20 mM Tris, pH 7.5, 150 mM NaCl for CD2AP SH3-1 or supplemented with 2 mM β-mercaptoethanol for CD2AP SH3-2 and -3). Purified protein was dialyzed against the final buffer (5 mM Tris, pH 7.5, for SH3-1; 5 mM Tris, pH 7.5, 2 mM β-mercaptoethanol for SH3-2 and SH3-3). Proteins were concentrated and quantified by UV absorption at 280 nm, and their integrity was checked by SDS-PAGE/Coomassie Blue staining.

Synthesis of Soluble Peptides and Microarrays

Apart from the RIN3 peptide permutation arrays, all arrays and soluble peptides were synthesized as described (25). RIN3 peptide permutation arrays were prepared on cellulose-(3-amino-2-hydroxypropyl)-ether membranes (26) using a SPOT robot (Intavis AG, Cologne, Germany) according to our standard spot synthesis protocol. The arrays were designed using in-house LISA software. Cellulose-(3-amino-2-hydroxypropyl)-ether membranes gave a better signal/noise ratio compared with standard β-alanine cellulose membranes (26, 27).

Peptide Array Far-Western Blots

CBL

Scanning Array—The entire human CBL protein sequence was spot-synthesized as 21-aa partially overlapping peptides, sliding 3 aa with each step. Membranes were prepared as described (28), briefly prewetted in ethanol, and then washed with TBST (20 mM Tris-HCl, pH 7.5, 100 mM NaCl, 0.1% (v/v) Tween 20) three times for 10 min and blocked in TBST with 5% (w/v) nonfat dry milk for 4 h at room temperature. Membranes were incubated with 0.56 μM (14 μg/ml) purified GST in blocking buffer overnight at 4 °C to detect any background signals elicited by the GST tag. After washing three times in TBST for 10 min, membranes were probed with an anti-GST mAb, washed again, and incubated with HRP-coupled secondary (anti-Ig) antibody. Membranes were then reblocked for 1 h after washing and reprobed with 0.56 μM (20 μg/ml) GST-CD2AP SH3 domain overnight at 4 °C. Bound GST-CD2AP SH3 was detected as described for GST; signals were apparent after several seconds.

Truncation Array—N- and C-terminally truncated peptides containing the 21-aa CBL epitope (GSQVPERPPKPFPRRINSERK) were spot-synthesized in duplicate and probed as described above.

Permutation Array—21-aa peptides encompassing the CBL epitope GSQVPERPPKPFPRRINSERK were permutated in single positions (underlined) to all 20 common amino acid residues, in duplicate rows, and probed as described above.

ALIX

Permutation Array—Spot-synthesized 21-aa peptides containing the ALIX epitope AGGHAPTPPTPAPRTMPPTKP were permutated in single positions (underlined) to all 20 other residues, in duplicate rows. Membranes were probed as above for the CBL permutation array.

Proteome-wide search for novel putative CD2AP SH3 binding partners

The P*x*P*x*PR motif in CBL was used as a search sequence for scanning the human proteome, disregarding splice variants, with *ScanProsite* (29). From 695 hits, a subset of 74 potential binding sites in 62 proteins with known or possible roles in signaling was selected; preference was given to proteins involved in membrane trafficking and/or signaling. Selected sequences were spot-synthesized on a microarray as 21-aa peptides, in duplicate. The arrays were probed as described for the CBL scanning array.

RIN3

Scanning Array—The entire human RIN3 protein sequence was spot-synthesized as partially overlapping 27-aa peptides, sliding 3 aa with each step. Three array copies were probed as described above for the CBL arrays, except 0.1 μM (2.6 μg/ml) GST or 0.1 μM (3.6 μg/ml) GST-SH3 was used in the same blocking buffer (TBST, 5% (w/v) nonfat dry milk).

Permutation Array—Two 17-aa sequences from RIN3 (AKKNLPTAPPRRRVSER and TAKQPPVPPPRKKRISR) that bind to CD2AP SH3 domains were permutated at 15 single positions (underlined) to 20 aa and spot-synthesized in single rows. Arrays were probed as for the RIN3 scanning arrays, except with a modified blocking buffer (2% (w/v) ovalbumin in RIPA-100, for GST-SH3-1 and -SH3-2, or supplemented with 2 mM DTT, for GST-SH3-3) partly due to the different membrane type. No background GST signal was detected after 2 min, whereas GST-SH3 signals appeared after 1 s.

ITC

ITC was performed at 25 °C with a VP-ITC microcalorimeter (MicroCal/Malvern Instruments) essentially as described (30), but peptides were dissolved at 0.75–1.5 mM, and protein solutions of CD2AP SH3-1, SH3-2, or SH3-3 domains were used at 0.05–0.1 mM in ITC buffer (25 mM HEPES, pH 7.5, 100 mM potassium acetate). An initial injection of 4 μl of peptide solution was followed by 18 15-μl injections into the sample cell containing protein solution. Background heats from injection of peptide into buffer solution without protein were subtracted from experimental heats and then analyzed in ORIGIN (version 5.0) software by fitting to a model for a single set of binding sites using χ^2 minimization.

Protein Crystallography

CD2AP SH3-1·RIN3e1 complex

The SH3-1 domain was mixed in a 1:3.5 ratio with a 16-mer RIN3e1 peptide (AKKNLPTAPPRRRVSE). Crystals were grown by vapor diffusion in a sitting nanodrop (total volume of 150 nl) at 20 °C from a 1:1 ratio of mother liquor (0.1 M calcium

acetate, pH 4.2, 0.2 M Li_2SO_4, and 25% PEG 10,000) to CD2AP SH3-1 protein solution (19 mg/ml). A cluster of needles (~160 μm long), which grew after 2 weeks, was transferred to cryoprotectant (mother liquor supplemented with 25% glycerol) before being snap-frozen in liquid nitrogen. Data were collected to 1.6 Å on beamline I04 at Diamond Light Source synchrotron (Harwell, UK). Data were reduced with the *XDS* package (31), converted to *CCP4* mtz format, and scaled with *SCALA* (32); data to 1.65 Å were kept for refinement. Molecular replacement was done in *PHASER* (33) using as a search model the SH3 domain alone from a reported binary complex of CD2AP SH3-1 and CBL-b peptide (PDB code 2J6F). The single, correct solution in space group C2 was refined with *REFMAC5* (34), and additional manual model building was done in *COOT* (35). TLS (torsion, libration, screw) restraints were included for six groups (*i.e.* each chain in the asymmetric unit) (three SH3-1 domains and three RIN3 peptides). The final model was generated by optimizing experimental data/geometry restraint weighting and refining the water structure in *PHENIX* (36) before deposition in the PDB under accession code 4WCI.

CD2AP SH3-2·RIN3e2 complex

The SH3-2 domain was mixed with a 16-mer RIN3e2 peptide (TAKQPPVPPPRKKRIS) in a 1:3 ratio. Crystallizations were set up as for the SH3-1·RIN3e1 complex. After 3 weeks, a single, thin, square plate (~180 μm in length/width) grew from a 2:1 ratio of mother liquor (0.1 M HEPES, pH 7.5, 1.4 M trisodium citrate dehydrate) to CD2AP SH3-2 protein solution (16.7 mg/ml). This crystal was transferred to cryoprotectant (mother liquor supplemented with 10% glycerol) and then snap-frozen in liquid nitrogen. Data were collected to 1.11 Å on beamline I03 at the Diamond synchrotron. Data were reduced with the *XDS* package, proving incomplete in most resolution shells (space group C2), so an additional data set was later collected using the same crystal but reoriented in the beam (Diamond beamline I04-1). The two data sets were merged with *XSCALE* before conversion to *CCP4* mtz format. Molecular replacement with *PHASER* used an ensemble of SH3 models homologous to CD2AP SH3-2 (PDB codes 2G6F, 1OEB, 2AK5, 2FEI, and 3IQL). The single, correct solution was subjected to automatic model building with *AutoBuild* in the *PHENIX* suite and later *REFMAC5* refinement. Additional manual model building was done with *COOT*. Anisotropic B-factors and several alternative conformations were included. The final model was deposited in the PDB with accession code 3U23.

Cell Culture

Conditionally immortalized human kidney podocytes were a kind gift from Prof. Moin A. Saleem (University of Bristol). Podocytes were maintained in RPMI 1640 medium supplemented with 10% FBS and 1% ITS (insulin-transferrin-selenium) and incubated at 33 °C with 5% CO_2. Differentiation was triggered by thermo-switching to 37 °C as described (37). HEK293 and HepG2 cell lines were grown in DMEM supplemented with 10% FBS and 1% penicillin/streptomycin and incubated at 37 °C with 5% CO_2. Jurkat cells were cultured in RPMI 1640, 10% FBS at 37 °C with 5% CO_2. Growth medium was changed every 2–3 days. Cells were split at a ratio of 1:3 to 1:5 when they reached 80–90% confluence by washing with PBS and incubating for <5 min with 1–2 ml of 0.25% trypsin, 0.1% EDTA in PBS solution until the cells detached before centrifuging at 200 × *g* for 5 min and resuspending in fresh medium. MCF10A cells were grown as described (38) without antibiotics.

Western Blotting, Immunoprecipitations, and Pull-downs

Total cell lysates were prepared and analyzed by Western blotting essentially as described (39). For immunoprecipitation of wild-type human RIN3 and CD2AP, HEK293T cells were transiently co-transfected with 0.5 μg each of FLAG-tagged CD2AP and Myc-tagged RIN3 per 60-mm dish using FuGENE-6 and then lysed in HNTG buffer (50 mM Hepes, pH 7.4, 150 mM NaCl, 1% Triton X-100, 10% glycerol, 10 mM EDTA) with 1 mM PMSF, 1 mM aprotinin, and 1 mM leupeptin added. Washed GammaBind™ G-Sepharose™ beads (GE Healthcare) were then added to the samples for 90 min at 4 °C. Immunoprecipitates were washed four times with ice-cold HNTG buffer containing 0.1% Triton X-100 plus inhibitors as above and then subjected to Western blotting with specific antibodies (Abs). Monoclonal Abs were used against c-Myc (clone 9E10, sc-40, Santa Cruz Biotechnology, Inc.) and FLAG (M2, Sigma-Aldrich), and a polyclonal rabbit Ab was used against CD2AP (sc-9137, Santa Cruz Biotechnology).

For GST pull-downs, equal amounts of purified GST fusion proteins (GST-CD2AP SH3 domains; GST-RIN3(378–467)) were coupled to reduced glutathione-Sepharose beads (GE Healthcare) and incubated with 1 mg of total cell radioimmune precipitation assay protein extract for 16 h with rocking at 4 °C, followed by three 1-ml washes with chilled RIPA-100 buffer (20 mM Tris-HCl, pH 7.5, 1 mM EDTA, 1% Triton X-100, 0.5% sodium deoxycholate, 0.1% SDS, and 100 mM NaCl). Proteins were separated by SDS-PAGE followed by semidry transfer onto polyvinylidene difluoride (PVDF) membranes (Hybond-P, GE Healthcare) and then blocked, probed, and developed as described (40). The anti-CBL mouse monoclonal Ab (A-9) was from Santa Cruz Biotechnology (sc-1651). The anti-RIN3 antibody (41) was kindly donated by Prof. John J. Colicelli (UCLA, Los Angeles, CA).

Immunofluorescence

MCF10A cells plated on poly-L-lysine-coated coverslips were transfected with GFP-RAB5a, FLAG-CD2AP, RFP-RIN3, and RFP-RIN3mut. The next day, cells were washed, fixed with 2% formaldehyde-PBS for 10 min at room temperature, and permeabilized with 0.2% Triton X-100/PBS for 1 min. Cells were stained with monoclonal anti-FLAG antibody (M2, Sigma; 1:50,000) diluted in PBS-Triton (0.02%). After four washes, cells were incubated with Alexa647-goat anti-mouse IgG (Molecular Probes, Inc.; 1:500).

Results

Analysis of the Interaction between the First Two CD2AP SH3 Domains and CBL—CD2AP SH3-1 and SH3-2 bind to a known region in the C terminus of CBL (7, 16, 42) and participate in the linkage of EGF receptor internalization to the cytoskeleton. We

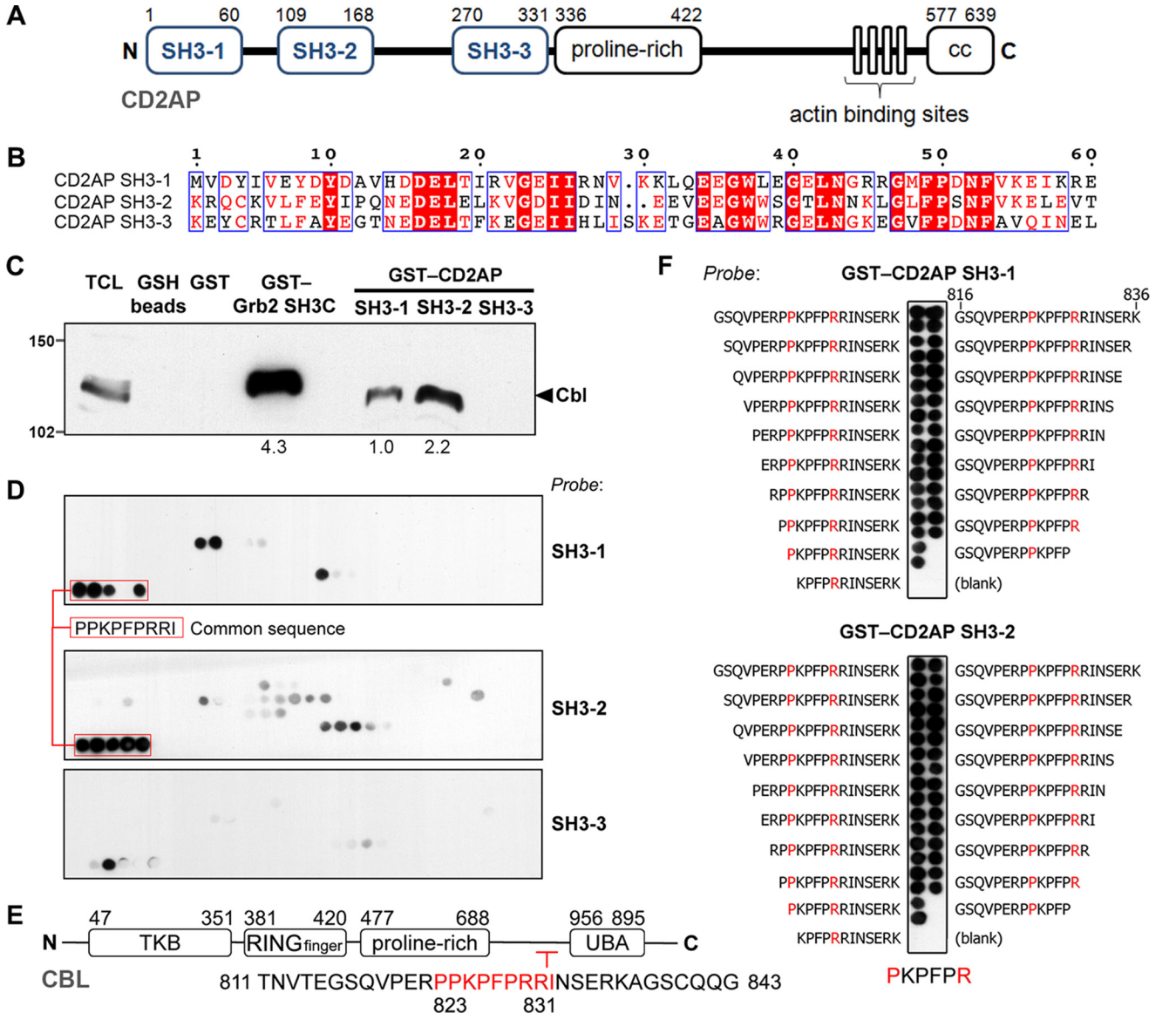

FIGURE 1. **CD2AP SH3-1 and SH3-2, but not SH3-3, bind directly to CBL via a motif bounded by Pro-824 and Arg-829.** *A*, schematic CD2AP domain composition. *SH3*, Src homology 3; *proline-rich*, proline-rich region; *CC*, coiled-coil domain; an actin binding region is shown with putative interaction sites. *N* and *C* represent the protein termini. *B*, sequence alignment of the human CD2AP SH3 domains. Identical residues down columns are shown as *red boxes* with *white letters*. Residues that have higher than 70% similarity (based on physico-chemical properties) in a column are shown as *red letters* in *blue frames*. The highest pairwise sequence identity is found between SH3-2 and SH3-3 (45%); SH3-1 and SH3-2 have less identity (40%); SH3-1 and SH3-3 have the lowest identity (38%). *C*, GST pull-downs. 1 mg of Jurkat total cell lysate was precipitated with 50 μg of bead-immobilized GST or GST-SH3 fusion proteins; precipitates were immunoblotted with an anti-CBL antibody. Values from densitometry *below* the blot show the CBL signal after pull-downs with each GST-SH3 relative to the intensity for CD2AP SH3-1. *D*, peptide scanning arrays. On cellulose membranes, peptides were spot-synthesized as overlapping 21 aa, sliding 3 aa with each step to cover the full human CBL sequence. Membranes were initially probed with 0.1 μM GST before immunodetection to confirm no nonspecific binding and then washed, reblocked, and probed again with 0.1 μM GST-CD2AP SH3-1, GST-CD2AP SH3-2, or GST-CD2AP SH3-3, as described under "Experimental Procedures." The series of spots that gave the strongest signals are *boxed* in *red*. *E*, schematic domain composition of human CBL. The full sequence region spanned by the *boxed* series of spots in *D* (aa 811–843) is shown. The portion of this sequence common to each spot in the series, encompassing the CD2AP SH3 recognition sequence, is shown in *red letters*. *TKB*, tyrosine kinase binding domain; *RING finger*, really interesting new gene zinc finger domain; *proline-rich*, proline-rich region; *UBA*, ubiquitin-associated domain. *F*, truncation arrays. N- and C-terminally truncated peptides of the 21-aa CBL epitope were spot-synthesized in duplicate. Arrays were first probed with GST and then GST-CD2AP SH3-1 or GST-CD2AP SH3-2 as described in *D*. Truncation beyond Pro-824 and Arg-829 (*colored* in *red*) prevents binding, which identified the core motif boundaries.

confirmed these interactions in Jurkat cells by showing that both CD2AP SH3-1 and SH3-2 could pull down CBL, but the third SH3 domain could not (Fig. 1*C*). Interestingly, SH3-2 was more effective than SH3-1, pulling down over twice the amount of CBL, suggesting a stronger interaction. The adaptor protein Grb2, cooperating with CBL, is indispensable for EGF receptor internalization (43) and may bind to CBL via both its N- and C-terminal SH3 domains (44),[9] so we compared the latter interaction in our experiment. We found that Grb2 SH3C pulled down twice the amount of CBL compared with CD2AP SH3-2 (Fig. 1*C*). This suggested that the interaction of CBL with

[9] E. Rouka, P. C. Simister, M. Janning, M. Lewitzky, J. Kumbrink, K. H. Kirsch, and S. M. Feller, unpublished results.

CD2AP might be less dominant in EGF receptor endocytosis than the Grb2-mediated interaction, similar to the minor or redundant role reported for the CD2AP homologue CIN85 (43). We then validated *in vitro* the interactions of all three CD2AP SH3 domains with CBL (42) to confirm whether the C-terminal binding site was unique. Thus, with each SH3 domain as a GST fusion, we probed spot-synthesized CBL peptide scanning arrays of peptides that covered the entire human CBL sequence. We found that the C-terminal epitope is indeed the major specific binding site for SH3 domains 1 and 2 and, to a much lesser extent, also SH3-3 (Fig. 1, *D* and *E*). To determine the boundaries of the CBL epitope, we used arrayed CBL peptides (aa 816–836) sequentially truncated from either the N or C terminus and probed with the first two CD2AP SH3 domains (as GST fusions). The recognition motif extended from Pro-824 to Arg-829 in CBL (Fig. 1*F*). Membranes first probed with GST alone as a control gave no background signal in an equivalent exposure time (data not shown).

Although Arg-829 has been identified as a critical residue for the interaction of CBL with CD2AP SH3-1 and SH3-2 (42), we aimed to map comprehensively the exact residues required for binding. First, we quantified the interactions of the three CD2AP SH3 domains with CBL by ITC (Table 1). We found that SH3-2 bound most strongly (K_d = 6.7 μM), whereas SH3-1 and SH3-3, respectively, bound 2.7- and 21-fold more weakly compared with SH3-2. These results reflected the differences observed in GST pull-downs (Fig. 1*C*) and the scanning array (Fig. 1*D*).

TABLE 1

Binding affinities of CBL and ALIX peptides to each CD2AP SH3 domain

Data were obtained by ITC. See legend to Table 2 for the color map key, and see supplemental Table S1 for more details.

Protein	Peptide sequence	Length (a.a.)	K_d ± SE (μM)		
			SH3-1	SH3-2	SH3-3
CBL	GDPTTNVTEGSQVPERPPKPFPRRINSE	28	**17.5** ± 1.7	**6.5** ± 0.5	**137.0** ± 7.3
ALIX	AGGHAPTPPTPAPRTMPPTKP	21	**6.6** ± 0.002	**4.2** ± 0.001	**32.2** ± 1.9

To explore the CBL motif in greater detail and to study any similarities and differences in the binding modes of the first two CD2AP SH3 domains, we probed spot-synthesized 20-aa permutation arrays of the CBL epitope (Fig. 2). Both CD2AP SH3-1 and SH3-2 recognized a core $P^1xP^3xP^5R^6$ motif in CBL (superscript numbers refer to relative motif positions, and *x* indicates that the residue position is unimportant for the interaction; this notation is used throughout). The array also detected some degree of selection for the interaction in motif positions 2 and 4, most notably for SH3-2, giving P*x*PfPR (or possibly PkPfPR) as the full recognition sequence (lowercase letters denote less important residues for the interaction; Fig. 3). This sequence is, in part, similar to one previously reported highlighting a minor role for the equivalent Lys in CBL-b, which permitted binding to CD2AP SH3-1 in two orientations as heterotrimers (45). In our peptide array a K825A substitution reduced the binding signal, consistent with the reported effect of a CBL-b K907A mutation (45). However, binding between CBL and every CD2AP SH3 domain in ITC experiments had 1:1 stoichiometry, implying that each complex was heterodimeric (supplemental Table S1 and Fig. S1). Interestingly, the array revealed that an alanine in motif position 3 was equally acceptable in the case of both SH3-1 and SH3-2 binding, whereas SH3-2 tolerated additional residues in two other peptide positions. This suggested that CD2AP may also bind a P*x*A*x*PR motif.

Bioinformatics and in Vitro Screens Identified 40 Putative CD2AP SH3-interacting Proteins—We investigated how frequently the CBL P*x*P*x*PR motif featured in the human proteome in order to discover other CD2AP-interacting proteins. A proteome search using the *ScanProsite* Web tool (29) yielded 602 proteins (695 sequence hits in total) containing this motif. We filtered these hits to prioritize cytosolic signaling proteins,

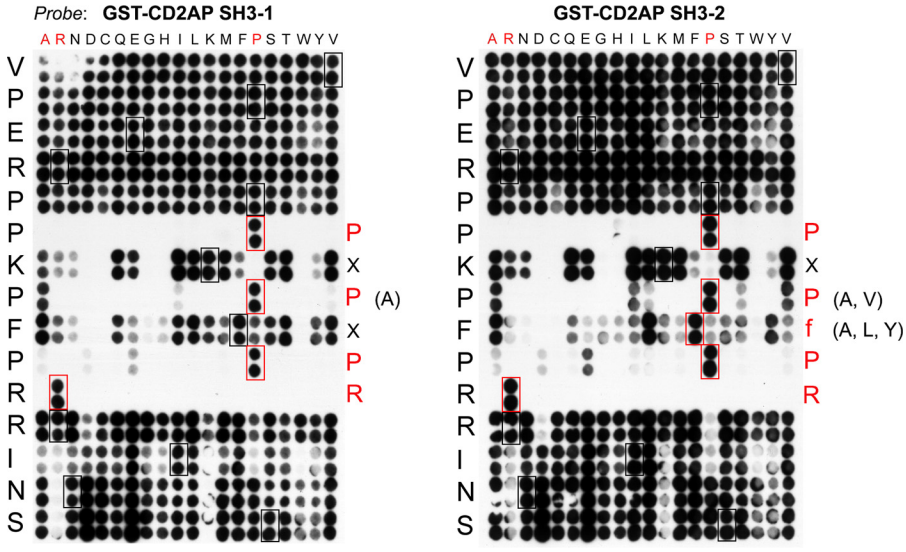

FIGURE 2. **CD2AP SH3-1 and SH3-2 recognize a P*x*P*x*PR motif in CBL.** 21-aa peptides of the CBL epitope GSQVPERPPKPFPRRINSERK were permutated in single positions (underlined) to the 20 common residues, in duplicate rows. Arrays were initially probed with GST and then with GST-CD2AP SH3-1 or GST-CD2AP SH3-2, as described for Fig. 1*D*. The CBL peptide sequence, and hence each residue position permutated, is displayed *vertically down* the *left side* of each array; the individual amino acid substitutions at these positions are listed *across* the *top*. Wild-type CBL peptide spots are *boxed*; those emphasized in *red boxes* show highly restricted positions (*i.e.* key motif determinants). Note that the amino acid preferences at these positions are further highlighted on the *right side* of each array. *Lowercase red type* indicates less critical positions; a *black letter x* marks unimportant positions within a motif. *Red type*, wild-type sequence; *smaller black type (capital letters)*, amino acids giving a signal intensity similar to wild type.

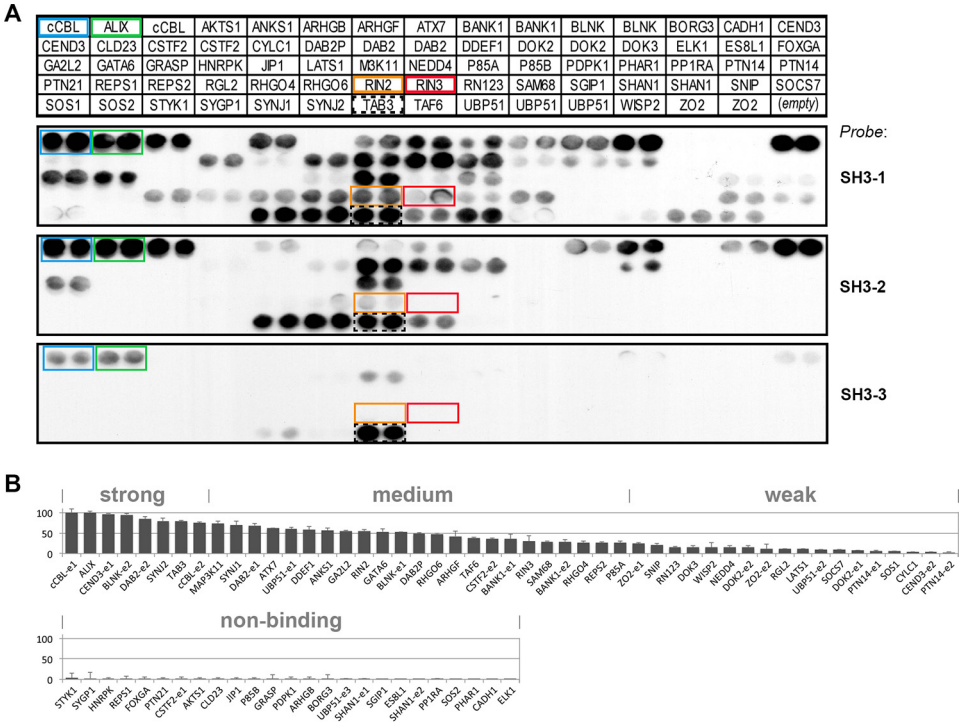

FIGURE 3. **Peptide array motif screen identifies 40 candidate CD2AP SH3 binding partners.** *A*, a list of nearly 700 human proteins harboring a P*x*P*x*PR motif as in CBL were identified using ScanProsite (29) and filtered according to presumed biological functions to give 74 different epitopes within 62 candidate binding partners for further analysis. These were spot-synthesized as 21-aa peptides on cellulose membranes, in duplicate (see Table S1). Some known binders were also included (*e.g.* CBL as a positive control and ALIX). Three array copies were initially probed with GST and then with either GST-CD2AP SH3-1 (*second panel from top*), GST-CD2AP SH3-2 (*third panel*), or GST-CD2AP SH3-3 (*bottom panel*), as described for Fig. 1*D*. The *top panel* depicts the array positions of all hit peptides tested. Spots corresponding to CBL, ALIX, RIN2, and RIN3 peptides are *boxed* in *blue*, *green*, *orange*, and *red*, respectively; TAB3 peptides have a *black box* (*dashed line*). *B*, densitometric analysis of duplicate-mean spot signals was done to rank the intensities normalized to the strongest signal from the CBL control (expressed as the 100% level) and thus broadly to classify binders according to their relative binding strengths, as follows: strong (>75%), medium (25–75%), or weak (<25%). Strong binders included ALIX, BLNK, CBL, CEND3, DAB2, SYNJ2, and TAB3. Medium-strength binders (25–75% of the CBL control signal) comprised ANKS1, ARHGF, ATX7, BANK1, CSTF2, DAB2P, DDEF1, GA2L2, GATA6, MAP3K11, P85A, REPS2, RHGO4, RHGO6, RIN2, RIN3, SAM68, SYNJ1, TAF6, and UBP51. Low intensity binders (<25% of the control signal) were CYLC1, DOK2, DOK3, LATS1, NEDD4-like, PTN14, RGL2, RN123, SNIP, SOCS7, SOS1, WISP2, and ZO-2. Non-binders, taken to be those spots not visible to the naked eye, had a mean signal of <3% of CBL. Proteins that did not bind with a single epitope to any CD2AP SH3 were AKTS1, ARHGB, BORG3, CADH1, CLD23, ELK1, ES8L1, FOXGA, GRASP, HNRPK, JIP1, P85B, PDPK1, PHAR1, PP1RA, PTN21, REPS1, SGIP1, SHAN1, SOS2, STYK1, and SYGP1.

ensuring the inclusion of those involved in membrane trafficking. Thus, 74 epitopes within 62 different proteins were selected for *in vitro* analysis by peptide microarray. These included a few reported partners (*e.g.* CBL and ALIX), useful as positive controls, but the majority were unknown as interactors. 21-residue peptides spanning the motif regions from these selected hits (supplemental Table S2) were spot-synthesized in duplicate on cellulose membranes, and three array copies were probed with one of each of the CD2AP SH3 domains (Fig. 3). Strikingly, the pattern of identified peptides binding to each SH3 was non-identical, with the proportion of hits as follows: 66% for SH3-1, 34% for SH3-2, and 9% for SH3-3. Note that in this analysis, we included all positive blotting reactions, however weak, because the intensity levels from probing immobilized peptides unoptimized for length and boundary positions are not always a reliable predictor of binding affinity in solution (46). Nevertheless, with the exception of CADH1, unique to SH3-2, the hits for SH3-2 formed an exact subset of those to which SH3-1 bound, and similarly for SH3-3, albeit a far smaller subset. Importantly, this third domain not only bound very few of the sequences, but also much more weakly, and thus appears poorly optimized for binding the core P*x*P*x*PR motif. This implies that SH3-3 may have different and as yet unidentified binding preferences and a divergent functional role. In total, peptides from 40 potential or known CD2AP-binding proteins were identified in the screen (disregarding TAB3; see below).

Differential Interactions of Each CD2AP SH3 Domain with an ALIX Peptide—The signal intensity of the CBL peptide spot, the strongest binder, was normalized to 100%, and all others were adjusted relatively based on densitometric analysis. Thus, other strong binders (>75% of the CBL signal) included ALIX, BLNK (SLP-65), CEND3, DAB2, SYNJ2, and TAB3. We were initially intrigued by TAB3 (Fig. 3, *dashed black boxes*) because it gave an intense signal with all three SH3 domains. However, full-length TAB3 scanning arrays revealed that this was a false positive hit, because nothing bound when DTT was included in the incubation buffer (data not shown). This was presumably due to a reactive cysteine in the TAB3 peptide with a propensity to form disulfide bonds with the GST-CD2AP SH3s, unlike other Cys-containing peptides in the original array, most of which did not bind (Fig. 3).

Next, we focused on ALIX (also called AIP1 or PDCD6IP), a component of the ESCRT (endosomal sorting complex required for transport) machinery. ALIX is a known CD2AP interactor (47), but the exact molecular determinants of binding have not been comprehensively elucidated. We found that

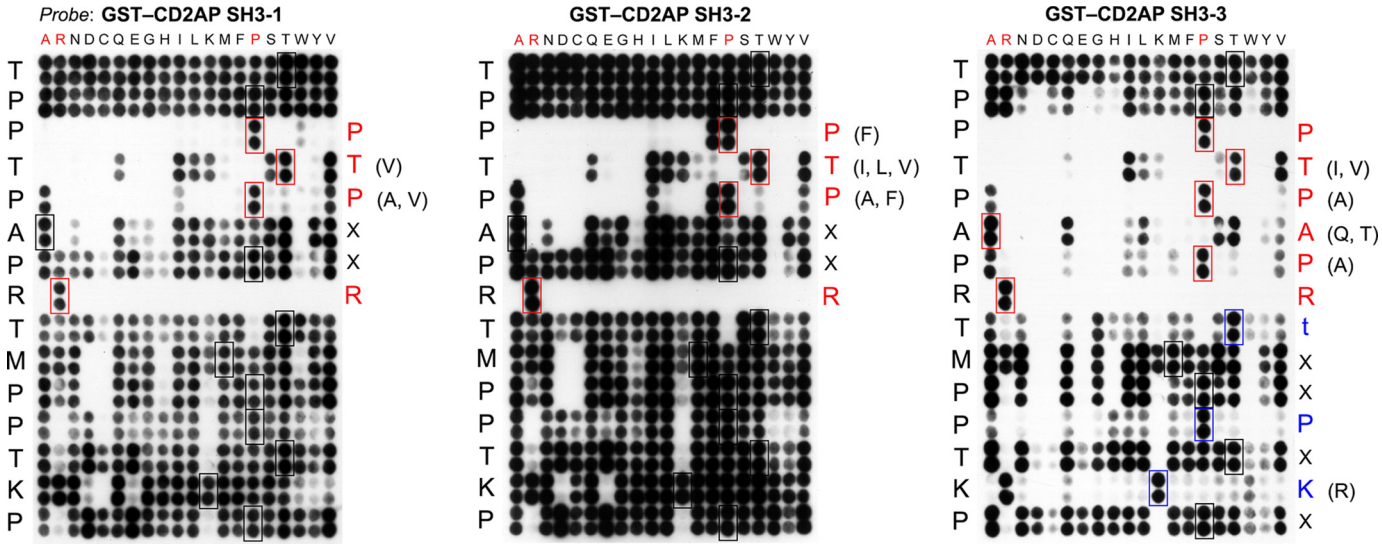

FIGURE 4. **CD2AP SH3-3 recognizes an extended epitope in ALIX unlike domains 1 and 2.** 21-aa peptides of the ALIX epitope AGGHAPTPPTPAPRTMPPTKP were permutated in single positions (underlined). The arrays were probed as described for Fig. 1*D* using GST-CD2AP SH3-1 (*left*), GST-CD2AP SH3-2 (*middle*), or GST-CD2AP SH3-3 (*right*). Wild-type ALIX peptide spots are *boxed*, and all other figure labeling is the same as for the CBL arrays (Fig. 3) except that *blue type* and *boxes* in the array probed with SH3-3 indicate additional restricted residue positions in an extended ALIX motif, not seen with SH3-1 or -2.

the ALIX epitope interacted with all three SH3 domains. ITC measurements with a synthesized 21-residue ALIX peptide and each SH3 revealed stronger binding to the first two SH3 domains (K_d values of 6.6 and 4.2 μM, respectively) compared with 5–8-fold lower affinity for SH3-3 (Table 1).

To explore the ALIX interaction in greater detail, we synthesized 20-aa permutation arrays based on the ALIX epitope (Fig. 4). Broadly, the array blotting patterns with SH3 domains 1 and 2 were very similar, but domain 3 displayed significant variation, again highlighting its distinct properties. Interestingly, the array data revealed that the first two domains recognize the motif PtP*xx*R. This differs in two key aspects from the CBL epitope: (i) Pro in position 5 of the CBL motif P^1xPxP^5R was surprisingly not a strict requirement according to the array yet was present in the ALIX motif; (ii) the second position is more restricted than in the CBL motif, mainly preferring a Thr as present in ALIX. Aliphatic residues (*i.e.* Val, Ile, Leu, and Lys (as found in CBL)) also permitted varying levels of binding.

Furthermore, we note that in position 3, Pro can be substituted by Ala without loss of binding affinity for both domains 1 and 2, as observed for the CBL motif (Fig. 2). Val (with SH3-1) and Phe (with SH3-2) substitutions in position 3 of the ALIX motif did not appear to alter the interaction strength either. Similarly, Phe in motif position 1 may substitute Pro to allow SH3-2 binding, unlike with SH3 domains 1 and 3. With respect to the SH3-3 binding preferences, the preferred motif according to the array is P^1tPaPRt*xx*P*x*K^{12} (Fig. 4, *right*). This is an unusually long recognition sequence compared with known CD2AP SH3 interaction motifs. Similar to domains 1 and 2, SH3-3 strictly required Pro in position 1, Arg in position 5, and Pro in position 3 (with Ala demonstrably possible). However, we observed a marked difference with SH3-3 in position 10, where proline was necessary for a strong interaction, and in position 12, a basic residue was essential (Lys in ALIX). This indicates that a patch beyond the canonical binding groove may be accessible for full interaction with SH3-3. However, SH3-3 still bound with lower affinity than SH3-1 and -2 to the ALIX peptide (K_d = 32 μM; Table 1), as observed with the CBL peptide (and RIN3e1; see below). The arrays gave no background signal when first probed with GST alone (data not shown).

RIN3 Is a Novel Interaction Partner for the CD2AP SH3 Domains in Kidney Cells—We also considered medium-intensity spots from the peptide array screen as useful hits because boundary positions may have influenced the signal strengths observed for the array peptides in immobilized form. Thus, the two RIN (Ras and Rab interactor) family proteins, RIN2 and RIN3, were analyzed further. Note that low intensity binders (<25% of the control signal) may also be relevant but were not pursued further. The RIN proteins were of special interest due to their link to endocytic processes, as guanine nucleotide exchange factors for the small GTPase RAB5, and hence potential candidates of physiological interplay with CD2AP; also, relatively little was known about their biological roles. Both RIN2 and RIN3 displayed noticeable binding to SH3-1, very weak binding to SH3-2, and yet no discernible binding to SH3-3 (Fig. 3). Therefore, to test the relevance of these interactions with full-length proteins, we used a co-immunoprecipitation system in HEK293 kidney cells with Myc-RIN2 or -RIN3 and FLAG-CD2AP. In contrast, there was barely a detectable interaction between CD2AP and RIN2 (data not shown), whereas a CD2AP·RIN3 complex could be co-immunoprecipitated (Fig. 5*A*). To determine the contribution of each SH3 domain to the RIN3 interaction, we carried out pull-down experiments using GST fusions of each individual SH3 domain and lysates from immortalized kidney podocytes. Only very low levels of endogenous RIN3 were detectable in undifferentiated cells (33 °C); increasing the temperature to 37 °C to trigger differentiation marginally increased RIN3 levels after 6–14 days (Fig. 5*B*; result at day 10 shown). We detected only limited bound RIN3 amounts in pull-down experiments with undifferentiated podocytes, but after cell differentiation, substantially more RIN3 was pulled down (Fig. 5*B*). SH3 domains 1 and 2 bound

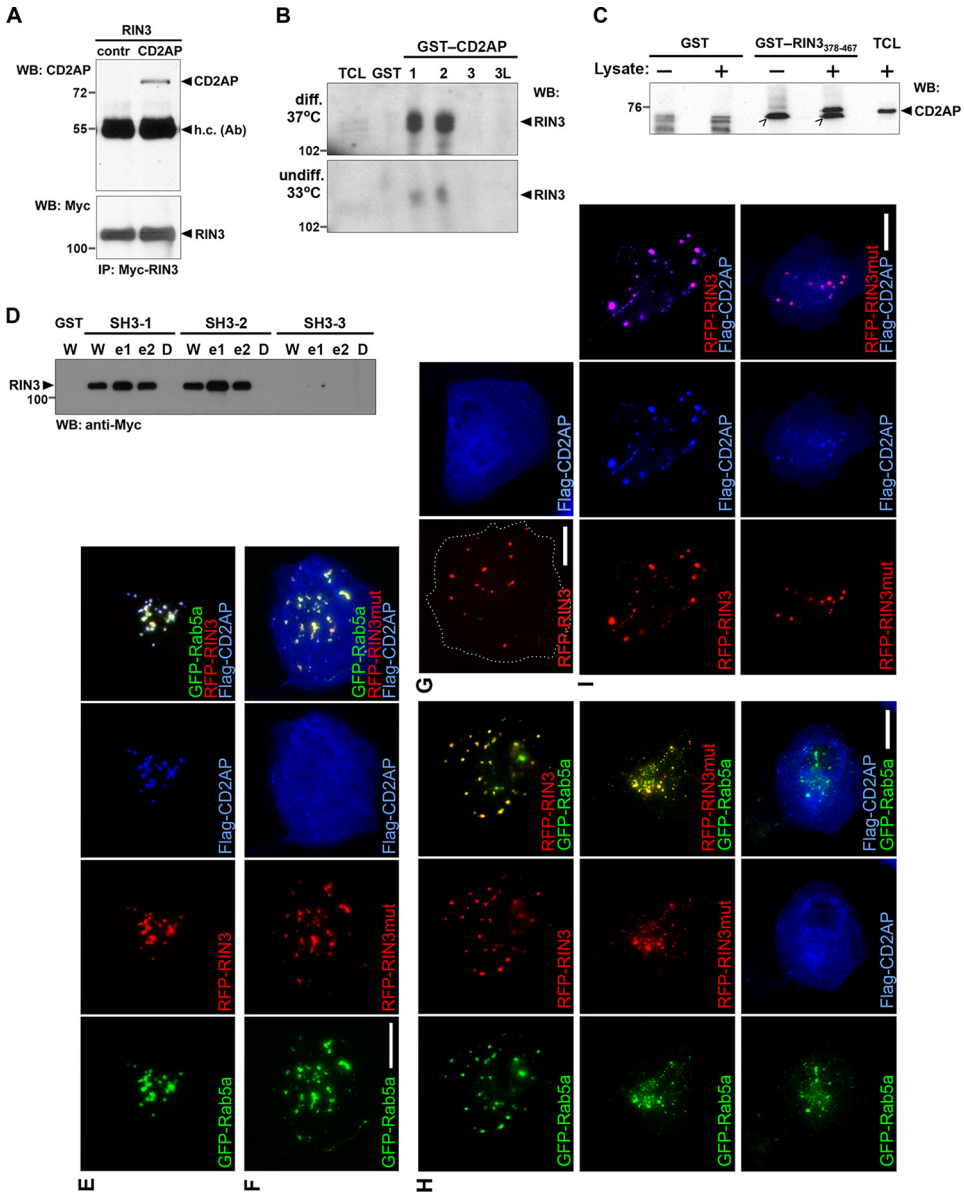

FIGURE 5. **RIN3 forms a complex with CD2AP in kidney cells, requiring SH3-1 and -2 only, and recruits it to RAB5a-positive endosomes.** *A*, co-immunoprecipitation of FLAG-CD2AP and Myc-RIN3 expressed in HEK293T cells. *B*, endogenous RIN3 in podocytes after 10 days of differentiation is pulled down by GST fusions of CD2AP SH3-1 and -2 (*lanes 1* and *2*, respectively) but neither SH3-3 (*lane 3*) nor a longer form of SH3-3 (*lane 3L*). RIN3 levels are very low in undifferentiated cells, and much smaller amounts are visible in the pull-down. *C*, in a reciprocal experiment, a GST-RIN3 construct encompassing both RIN3 epitopes (GST-RIN3(378–467)) can pull down endogenous CD2AP (compare *last two lanes*); however, GST alone cannot. Note that *open arrowheads* point to cross-reactivity of the anti-CD2AP antibody with the recombinant GST-RIN3 fusion protein (with or without lysate), also seen more faintly in the *GST-only lanes*. *D*, GST-CD2AP SH3 pull-downs with each SH3 domain and transfected full-length RIN3 as wild-type (*W*) or with non-binding mutated epitope 1 (*e1*) or 2 (*e2*) or both epitopes doubly mutated (*D*) from HEK293 cells. Both epitopes functionally bind to SH3-1 or -2, as the double RIN3 epitope mutants uniquely prevent a pull-down signal. See "Experimental Procedures" for further details. *WB*, Western blot; *TCL*, total cell lysate; *IP*, immunoprecipitation. *E–I*, MCF10A cells were transiently transfected to express tagged variants of RAB5a, RIN3, and CD2AP as indicated. Wild-type RIN3 recruited CD2AP to RAB5a-positive early endosomes (*E*), whereas a RIN3 variant in which the CD2AP binding sites were mutated (*RIN3mut*) failed to recruit CD2AP (*F*); *scale bar*, 15 μm. *G*, single expression revealed cytosolic localization for CD2AP and punctate localization for RIN3; *H*, co-expression of RAB5a demonstrated that both wild-type and mutant RIN3 (*RIN3mut*) localized to early endosomes but that CD2AP did not; *scale bars*, 15 μm. *I*, wild-type RIN3 recruited CD2AP into the punctate structures, whereas RIN3mut only showed minimal co-localization with CD2AP; *scale bar*, 10 μm.

equal amounts of RIN3, but SH3-3 failed to elicit a positive pull-down, as did the GST-only control. Recently, the SH3-3 domain from the homologue CIN85 showed greater thermal stability and expression yield compared with a shorter construct when its N and C termini were extended (48). Therefore, in case the negative SH3-3 pull-down result was somehow related to suboptimal boundaries of our GST-SH3-3 domain construct (should protein stability affect ligand binding), we generated a longer SH3-3 construct. This was extended at both termini in total by 10 residues, equivalent to the region elongated in CIN85 SH3-3 (48). However, the longer construct did not pull down RIN3 either (labeled *3L* in Fig. 5*B*), confirming the different behavior of SH3-3 relative to SH3-1 and -2.

RIN3 Harbors Two CD2AP Interaction Motifs—RIN3 has an extended PRR in its N-terminal half. Given the potential for

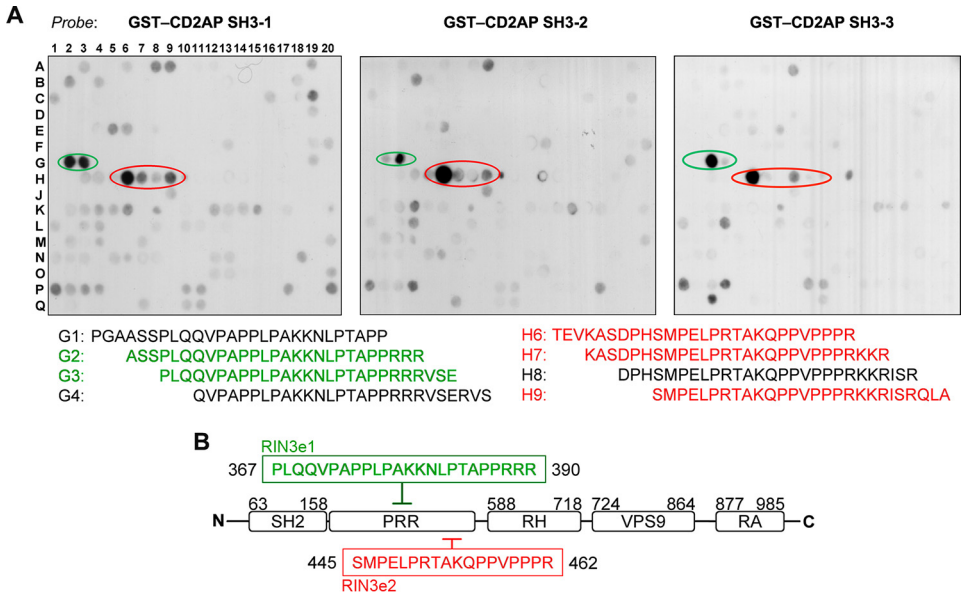

FIGURE 6. **Each CD2AP SH3 domain recognizes the same two RIN3 epitopes.** *A*, RIN3 scanning arrays. Overlapping 27-aa human RIN3 peptides were spot-synthesized on cellulose membranes sliding 3 aa with each step to cover the full protein sequence. Arrays were initially probed with GST and then with GST-CD2AP SH3-1 (*left*), GST-CD2AP SH3-2 (*middle*), or GST-CD2AP SH3-3 (*right*), as described for Fig. 1*D*. Two principal binding regions are evident (*ringed* in *green* and *red*). The exact sequence of each spot is found *below* the arrays (same *color coding*). Note that, unlike results obtained with CBL (Fig. 1, *D* and *F*), the actual RIN3 peptide boundaries appear to influence probe binding onto the arrayed peptides much more strongly. *B*, schematic domain composition of RIN3. The *boxed sequences* represent the minimal common segment found in all binding spots for that region (again, *green* for epitope 1, aa 367–390; *red* for epitope 2, aa 445–462). *SH2*, Src homology 2; *RH*, RIN homology; *VPS9*, vacuolar sorting protein 9; *RA*, Ras association. Note that only PRR-2 and -3 have affinity for CD2AP.

variant motifs suggested by differences in the binding preferences observed in the ALIX and CBL permutation arrays, we tested whether RIN3 contained additional CD2AP binding sites (Fig. 6). Spot-synthesized scanning arrays of peptides covering the entire human RIN3 sequence were probed with the three individual CD2AP SH3 domains (Fig. 6*A*). Interestingly, each SH3 domain showed some binding to the originally screened motif region (Fig. 6*B*, *red box*), but an additional RIN3 epitope recognized by all three SH3 domains was also identified (Fig. 6*B*, *green box*). It differs from the screened sequence by not containing an exact P*x*P*x*PR motif; rather, Ala is present in motif position 3. The lack of immunoreaction to a longer contiguous series of array peptides harboring the motif indicated that the peptide boundaries were indeed critical for binding to these epitopes in short peptide form (*cf.* CBL scanning array; Fig. 1*D*) and explains why the initial screening array peptides sometimes gave weaker signals for this hit (Fig. 3).

Having mapped two binding epitopes, herein referred to as RIN3e1 and RIN3e2, we created a GST-fused RIN3 construct that spanned both epitopes in order to perform the reciprocal pull-down of CD2AP from cell lysates. GST-RIN3(378–467) was able to pull down endogenous CD2AP, whereas no CD2AP band was present with GST alone (Fig. 5*C*). Note that extra blot bands were visible due to cross-reactivity of the anti-CD2AP antibody with species in the recombinant protein sample, as determined by a lysate-free control. We proceeded to characterize the CD2AP-RIN3 interaction with comprehensive biochemical and biophysical approaches.

Substitution Analyses Revealed Px(P/A)xpR in RIN3 as the Preferred Recognition Motif—First, to delineate the recognition motifs as for CBL and ALIX, we synthesized 20-aa permutation arrays of RIN3e1 and RIN3e2 peptides (Fig. 7) and probed them with each CD2AP SH3 domain. These arrays were synthesized on a different carrier material, and although the initial GST-only control probe gave no appreciable signal (data not shown), a higher background signal was observed from nonspecific membrane binding by the SH3 domains, particularly the RIN3e2 arrays. However, the results still allowed clear detection of specific interactions (Fig. 7). In general, the signal pattern was strikingly similar between all three SH3 domains (in contrast to the ALIX peptide arrays; Fig. 4). Indeed, the residues P*x*P*x*pR formed the general recognition motif in RIN3e2, with Thr in position 2 of some importance. In RIN3e1, the second proline (motif position 3) was replaced by alanine, thereby forming the basis for recognition of the related motif: P*x*A*x*pR. In fact, the peptide arrays revealed that in the sequence contexts of either RIN3 epitope, Ala or Pro are equally strong binders in position 3, as seen for ALIX and CBL. Val in this position is also tolerated, only slightly weakening the interaction. In contrast, in position 1, only Pro appears possible for a strong interaction with every SH3 domain because any other residue prevented or weakened binding. The effect was more pronounced with RIN3e1 than with RIN3e2. Arg in position 6 was strictly required for strong binding in all cases. Pro in position 5 of RIN3e1 was essential for binding to SH3-2 and SH3-3 although not SH3-1. The equivalent Pro, however, was generally preferred for the strong interaction of all SH3 domains with RIN3e2, although greater tolerances exist in this position.

Both RIN3 Motifs Are Necessary for Full CD2AP Interaction and Its Recruitment by RIN3 to RAB5a-positive Endosomes—The ability of each RIN3 motif in the context of the full-length protein to interact with CD2AP was next assessed using the HEK293T transfection system, with mutated RIN3 variants. Motifs in epitopes 1 or 2 were rendered non-functional by dual

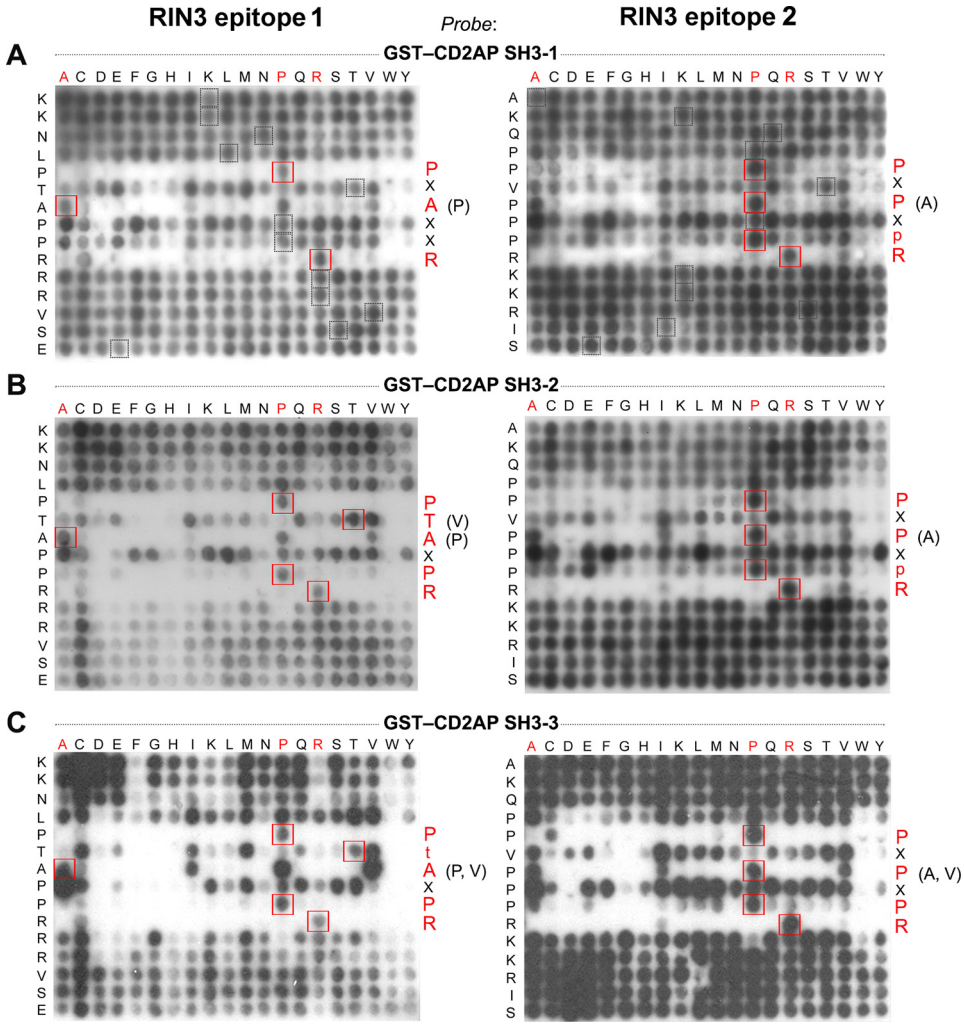

FIGURE 7. **All three CD2AP SH3 domains recognize variants of a Pt(P/A)xpR motif in RIN3.** The two RIN3 binding regions identified in the scanning array were spot-synthesized as 17-aa peptides on cellulose-(3-amino-2-hydroxypropyl)-ether membranes (RIN3e1, AKKNLPTAPPRRRVSER; RIN3e2, TAKQPPVPPPRKKRISR) and permutated in 15 single positions (underlined) against all 20 natural residues, in single rows. Three copies of the RIN3e1 permutation array (*all left panels*) or the RIN3e2 array (*all right panels*) were initially probed with GST as described for Fig. 1*D* and then with GST-CD2AP SH3-1 (*A*), GST-CD2AP SH3-2 (*B*), or GST-CD2AP SH3-3 (*C*). See also legend to Fig. 2 for an explanation of the array annotations.

Ala substitutions of the critical first and last motif positions (P*xxxx*R to A*xxxx*A); a third variant with both epitopes simultaneously mutated in this manner was also tested. Mirroring the previous result with endogenous RIN3 in podocytes (Fig. 5*B*), wild-type RIN3 (*W*) bound to SH3-1 and -2, but not SH3-3 or GST alone (Fig. 5*D*). Furthermore, whereas dual Ala substitutions in RIN3e1 or -e2 individually still allowed binding to the first two SH3 domains, indicating the independent functionality of each motif, only when both epitopes were mutated was binding prevented (double epitope mutant (*D*); Fig. 5*D*). The two binding sites may thus work in tandem for proper CD2AP interaction in the cell, engaging with the first two SH3 domains simultaneously.

Immunofluorescence microscopy was performed to investigate the association of RIN3 and CD2AP in transiently transfected cells in culture. In CD2AP-expressing cells, CD2AP is mainly localized in the cytoplasm and shows no obvious accumulation on RAB5a-labeled early endosomes (Fig. 5, *G* and *H*). As shown previously, RIN3 localizes to RAB5a-positive endosomes (Fig. 5*H*) (21). In addition, a RIN3 variant with the CD2AP binding sites mutated also targets to RAB5a-positive endosomes. Importantly, when RIN3 and CD2AP were co-expressed CD2AP became co-localized with RIN3 on early endosomes (Fig. 5, *E* and *I*). The recruitment of CD2AP to early endosomes was mediated by RIN3 because the RIN3 variant mutated for CD2AP interaction failed to recruit CD2AP to early endosomes (Fig. 5, *F* and *I*). These data revealed the importance of both RIN3 binding sites for interaction with CD2AP in cells.

ITC Data Confirmed Differences in CD2AP SH3 Interactions with Free RIN3 Peptides—To quantify binding, ITC experiments were performed between individual CD2AP SH3 domains (with GST tags cleaved off) and synthetic 16-mer RIN3e1 and RIN3e2 peptides (Table 2). In general, RIN3e1 binding affinities were comparable with those of the ALIX peptide, but RIN3e2 displayed tighter binding to all SH3 domains. Specifically, RIN3e1 bound to SH3-1 and SH3-2 with similar binding affinities (K_d values of 8.9 and 10.0 μM, respectively). Similar behavior was seen for RIN3e2 yet with even higher affinities (K_d = 1.6 and 2.1 μM). SH3-3, however, displayed about 4-fold weaker binding than SH3-1 to RIN3e1 only (K_d ~40 μM) but unexpectedly bound with

TABLE 2

Binding affinities of wild-type and mutant RIN3 peptides to each CD2AP SH3 domain

Data were obtained by ITC. Two wild-type RIN3 epitopes (e1 and e2) were tested, and mutant versions of RIN3e2, the tighter binder. Affinities are grouped by increasing red colour intensity; the stronger the shade of red, the higher the affinity (the lower the K_d value). Color groups represent K_d ranges in half-log (μM) increments (*e.g.* strongest red: >0 – 0.5 log K_d (μM) = K_d range of >1–3.16 μM). TLQ, too low for quantification (of accurate affinities); wt, wild-type sequence; point mutants of RIN3e2 are also shown.

RIN3 epitopes		Peptide sequence	Length (a.a.)	K_d ± SE (μM)		
				SH3-1	SH3-2	SH3-3
e1	wt	AKKNLPTAPPRRRVSE	16	**8.9** ± 0.2	**10.0** ± 0.2	**39.8** ± 0.1
		NLPTAPPRRR	10	**13.5** ± 0.1	**10.7** ± 0.3	**84.8** ± 0.3
e2	wt	TAKQPPVPPPRKKRIS	16	**1.6** ± 0.1	**2.1** ± 0.8	**6.7** ± 0.3
		KQPPVPPPRKK	11	**10.4** ± 1.3	**15.1** ± 0.9	**57.5** ± 0.06
	$P_{457} \rightarrow A$	TAKQPAVPPPRKKRIS	16	**126.0** ± 1.7	**19.9** ± 2.6	**68.0** ± 0.24
	$P_{459} \rightarrow A$	TAKQPPVAPPRKKRIS	16	**2.2** ± 0.3	**3.1** ± 0.4	**6.9** ± 0.02
	$R_{462} \rightarrow A$	TAKQPPVPPPAKKRIS	16	TLQ	TLQ	TLQ
	$R_{462} \rightarrow L$	TAKQPPVPPPLKKRIS	16	TLQ	TLQ	TLQ
	$R_{462} \rightarrow V$	TAKQPPVPPPVKKRIS	16	TLQ	**47.1** ± 0.05	TLQ
	$R_{462} \rightarrow I$	TAKQPPVPPPIKKRIS	16	TLQ	**42.7** ± 0.05	TLQ
	$I_{466} \rightarrow A$	TAKQPPVPPPRKKRAS	16	**1.9** ± 0.1	**1.6** ± 0.2	**11.8** ± 2.0

Kd range (in *log μM*)	Colour key
>0 to 0.5	
>0.5 to 1.0	
>1.0 to 1.5	
>1.5 to 2.0	
>2.0 to 2.5	
>2.5 (TLQ)	

more similar affinity to RIN3e2 (6.7 μM), the tightest binding so far observed for this domain. Shorter RIN3 peptide lengths, such as 10- or 11-mers, reduced binding affinity relative to 16-mers, an effect that was more pronounced for epitope 2 than epitope 1. Thus, additional contributions to the binding energy may derive from residues beyond the canonical motif.

Next, to confirm the importance of the three principal motif determinants, focusing on the tighter binder, RIN3e2, we synthesized mutant peptides and measured their interactions with each CD2AP SH3 domain by ITC (Table 2). Thus, we introduced alanine point mutations in place of Pro-457, Pro-459, and Arg-462 (*i.e.* motif positions 1, 3, and 6). The P457A mutant peptide greatly weakened binding, most notably in the case of SH3-1, resulting in a >30-fold reduction in affinity relative to the wild-type sequence (and nearly 10-fold with SH3-2; 16-fold with SH3-3). The R462A mutant abolished the interaction with each SH3 to unquantifiable levels, indicating its key role in recognition. However, the P459A peptide maintained binding in the low micromolar range with all SH3 domains, not too dissimilar from the wild-type peptide. This was expected, reflecting the functional interchangeability of Ala for Pro in motif position 3 observed in the peptide array. Finally, ITC data showed that each SH3-peptide interaction was predominantly enthalpically driven, as is common for SH3s, but the tighter binding RIN3e2 peptide had a more favorable entropic contribution (supplemental Table S1).

High-resolution Crystal Structures of Heterodimers Revealed a More Extended Class II Binding Mode with a CD2AP SH3-2·RIN3e2 Complex Compared with CD2AP SH3-1·RIN3e1—In parallel, we attempted co-crystallization of each SH3 domain in complex with peptides encompassing each wild-type RIN3 motif. We solved high-resolution structures of both CD2AP SH3-1 in complex with RIN3e1 to 1.65 Å (PDB code 4WCI), and SH3-2 in complex with RIN3e2 to 1.11 Å (PDB code 3U23) (Fig. 8 and Table 3). However, crystallization attempts with SH3-3 did not yield crystals in apo form or as a complex. Both CD2AP SH3 domains 1 and 2 display the familiar SH3 fold of a six-stranded β-barrel. In the SH3-1·RIN3e1 structure, three copies of the complex form the asymmetric unit in a triangular arrangement. Each complex is a heterodimer (*i.e.* 1:1 stoichiometry), consistent with the ITC result (supplemental Table S1). Differences between monomers include the positions of the N termini (specifically, the residues are vector artifacts conjoined to the SH3), which extend out from the domain proper and provide various crystal-packing contacts. In each complex, the RIN3e1 peptide forms a left-handed polyproline type II helix and binds to the SH3 in class II orientation. Pro-382, Ala-384, and Arg-387 from the RIN3e1 peptide (*i.e.* the essential residues of the P*x*A*x*pR motif) selectively dock into the two hydrophobic pockets and the negatively charged specificity pocket of SH3-1, respectively (Fig. 8, *A* and *C*, *left panels*). Furthermore, Pro-386 makes no contacts with the SH3 at all, as inferred previously by the array, although Pro in this motif position 5 within a CBL epitope is essential for binding (Fig. 2). Pro-386 therefore presumably serves an essential structural role within the polyproline type II helix.

The structure of the SH3-2·RIN3e2 complex was solved with a single binary complex in the asymmetric unit (*i.e.* 1:1 stoichiometry), again consistent with our ITC data. The heterodimer reveals a similar complementary fit with Pro-457, Pro-459, and Arg-462 from RIN3e2, in bonding distance to the SH3-2 domain and in class II orientation (Fig. 8, *A* and C, *right panels*). As with RIN3e1, the RIN3e2 peptide adopts a polyproline type II helical conformation, but four extra residues beyond the C-terminal end of the canonical motif were visible in the electron density maps. Ile-466 in motif position 10 lies within a distal hydrophobic patch, flanked by Val-141, Leu-154, and Leu-156 on SH3-2, implicating Ile-466 in the interaction (Fig. 8, *A–C*, *right panels*). This is consistent with the reduced affinity observed for an 11-mer RIN3 peptide truncated at Lys-464 (motif position 8) compared with the 16-mer co-crystallized (ITC data; Table 2). Thus, the RIN3 recognition motif for SH3-2 may be more extended (*i.e.* $P^1xPxpRxxxI^{10}$), so we analyzed this further by ITC. An I464A mutant peptide curiously had no major effect on the binding affinity for SH3 domain 1 or 2 (Table 2), a result that mirrored our peptide array data, but

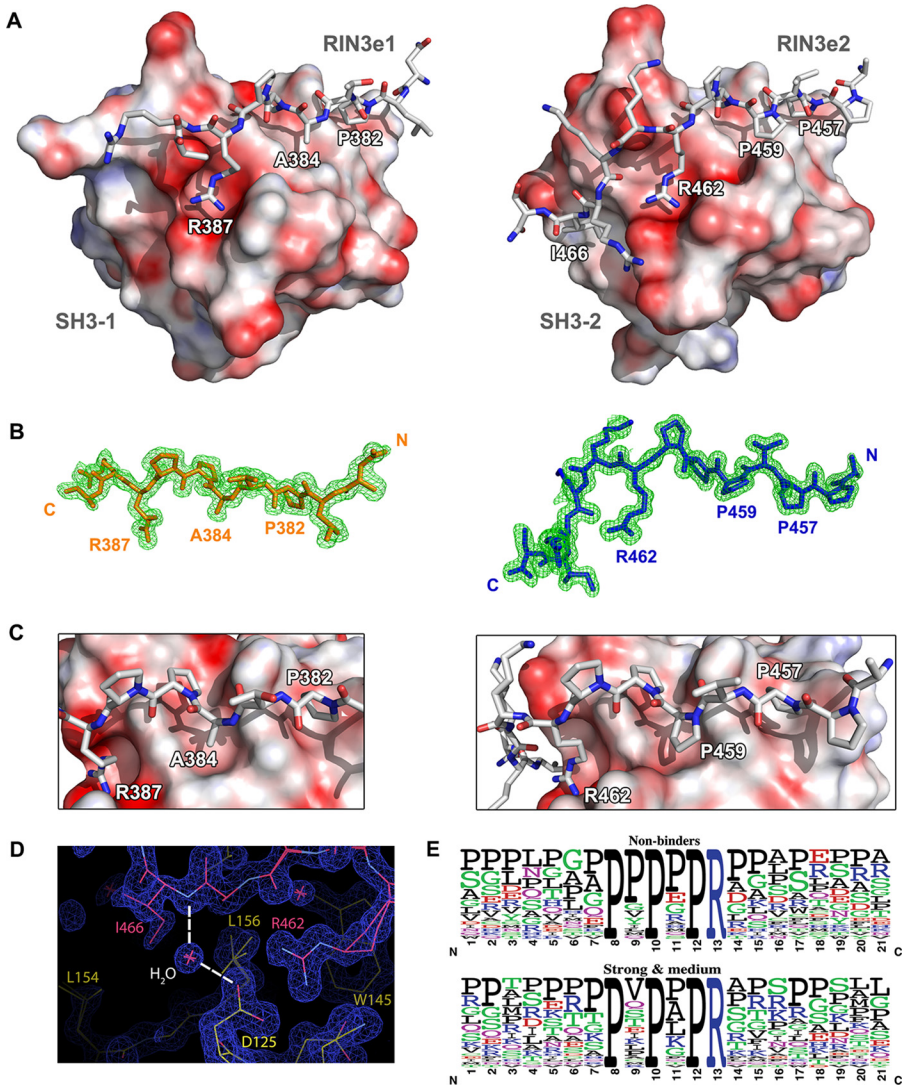

FIGURE 8. **Crystal structures of CD2AP SH3-1 and SH3-2 domains in binary complexes with RIN3 peptides.** CD2AP SH3-1 in complex with RIN3e1 (*left panels*) and CD2AP SH3-2 in complex with RIN3e2 (*right panels*) are depicted as follows. *A* and *C*, electrostatic potential surface representation; RIN3 peptides are shown in *stick representation* and *colored* by element (*white*, carbon; *blue*, nitrogen; *red*, oxygen). *C*, *close-up views* of RIN3 peptide docking. These two views were generated by rotating the view in *A* by −30° around the *y* axis, and 20° around the *x* axis. *B*, refined $2F_o - F_c$ electron density maps (*green mesh*) of docked RIN3 peptides (SH3 surface omitted) contoured at 1.0 electron/Å^3 illustrate the data quality. RIN3e1 (*orange sticks*) was modeled at 1.65 Å resolution (*left*), and RIN3e2 (*blue sticks*) was modeled at 1.11 Å resolution (*right*). RIN3 residues critical for the interaction are *labeled*. *D*, further detail of RIN3e2 (*pink sticks*) binding to SH3-2 (*yellow sticks*) within $2F_o - F_c$ electron density, a snapshot from the molecular graphics program *COOT* (35). Ile-466 docks onto a distal hydrophobic patch flanked by Val-141, Leu-154, and Leu-156 on the SH3 domain. A water oxygen atom (H_2O) stabilizes the interaction between the backbone amide nitrogen of Ile-466 in the RIN3e2 peptide and the SH3-2 residue Asp-125, which bonds to the key RIN3 motif residue Arg-462. The two alternative partial side-chain conformations of this Arg are visible. *E*, *Weblogos* of strong and medium binders from the P*x*P*x*PR array screen compared with non-binders (Fig. 3), created using the online tool (67).

weakened SH3-3 binding nearly 2-fold. However, inspection of the crystal structure indicated that a water molecule modeled with high confidence mediates hydrogen bonding between the main-chain nitrogen of Ile-466 in RIN3 and SH3-2 (Fig. 8*D*). In fact, it appears to stabilize Asp-125 in the SH3 domain, which participates in the key salt bridge to Arg-462 of the RIN3e2 recognition motif. This backbone hydrogen bond probably drives binding rather than the side chain, explaining the apparent discrepancy. Moreover, the extended interaction involving Ile-466 may contribute to the generally higher affinity of RIN3e2 to CD2AP SH3 domains than RIN3e1. Although the Ile side chain docked well on the hydrophobic patch, we acknowledge that crystal packing could have influenced its positioning.

In the SH3-2·RIN3e2 complex, SH3-2 Phe-117 and Phe-161 in the binding groove make hydrophobic contacts with RIN3 Pro-457, whereas Pro-459 interacts with SH3-2 Phe-161 and Tyr-119. RIN3 Arg-462 forms the characteristic salt bridge to SH3-2 Asp-125 and hydrophobic contacts with the aliphatic portion of its side chain along Trp-145 while also in polar bonding distance to Glu-126 and a backbone main-chain carbonyl oxygen in SH3-2. To evaluate the importance to SH3-2 Trp-145 binding of the hydrophobic portion of the RIN3 Arg-462 side chain, rather than electrostatic interaction with its guanidinium group, as shown previously for a Grb2 SH3 interaction (25), additional Arg-462 substitutions were tested by ITC. Arg was replaced by Ala, Ile, or Val, and the effects on binding were measured (Table 2). Typically, removal of the crucial salt bridge

TABLE 3

X-ray data collection, processing, and refinement parameters for two CD2AP SH3·RIN3 structural complexes

Values in parentheses represent the highest resolution shells. Molprobity values are those reported at the time of deposition. a.u., asymmetric unit.

Parameters	Complex 1	Complex 2
Structures deposited		
Protein/peptide	CD2AP SH3-1/RIN3e1	CD2AP SH3-2/RIN3e2
PDB code	4WCI	3U23
Data collection and processing		
Diamond Light Source beamline	I04	I03
Detector	Pilatus 2M	Pilatus 6M
Wavelength (Å)	0.9173	0.97625
Space group	C2	C2
Unit cell parameters		
a, b, c (Å)	95.53, 55.36, 64.56	53.13, 32.04, 39.18
α, β, γ (degrees)	90.00, 131.7, 90.00	90.00, 92.56, 90.00
Resolution range (Å)	48.19–1.65	27.43–1.11
Outer shell (Å)	1.74–1.65	1.2–1.11
Mean $I/\sigma(I)$	6.6 (2.4)	15.0 (2.9)
Completeness (%)	97.7 (93.0)	92.8 (74.5)
R_{merge} (%)	13.2 (47.9)	5.2 (34.1)
Refinement and validation		
R_{work} (%)	19.2 (27.8)	15.1 (33.7)
R_{free} (%)	21.9 (32.1)	16.7 (29.1)
Highest resolution bin (Å)	1.70–1.65	1.14–1.11
Root mean square deviation		
Bond angles (degrees)	1.01	2.27
Bond lengths (Å)	0.007	0.025
Ramachandran plot (%)		
Favored regions	98.61	98.31
Allowed regions	1.39	1.69
Outliers	0	0
Molprobity score; percentile	1.03; 100th	1.06; 97th
Additional data		
No. of binary complexes in a.u.	3	1

reduced binding between mutant peptide and SH3 to unquantifiable levels. However, the RIN3e2 R462V and R462I peptides retained significant interaction ability with SH3-2 uniquely (K_d = 47.1 and 42.7 μM, respectively), albeit with a >20-fold drop in affinity compared with the wild-type RIN3e2 peptide. Interestingly, the crystal structure captured two conformations of the aliphatic portion of the Arg-462 side chain within the negatively charged pocket (Fig. 8), which suggests that this essential residue nevertheless has flexibility in the bound state. In the SH3-1·RIN3e1 complex, RIN3 Pro-382 interacts with SH3-1 Tyr-8 and Phe-53; RIN3 Ala-384 interacts with Tyr-10 and Phe-53 in SH3-1; and Arg-387 forms the key salt bridge with SH3-1 Asp-15 and polar contacts with a main-chain oxygen and Asp-16 in SH3-1, whereas the aliphatic stretch of the Arg-387 side chain similarly makes hydrophobic contacts with SH3-1 Trp-37. No alternative conformation was seen for Arg-387.

Discussion

The multifunctional adaptor protein CD2AP binds multiple signaling partners. Through motif screening, we have identified further potential binders and characterized RIN3 as a novel, functional CD2AP interactor, co-recruited to RAB5a-positive endosomes. Although we report the first direct interaction, since this study began, both RIN3 and CD2AP have been implicated in the same "biological space" in several independent settings. First, two recent genome-wide association study reports based on single nucleotide polymorphism (SNP) data uncovered *CD2AP* as a novel highly associated risk factor gene in LOAD (19, 20), and later *RIN3* from a meta-analysis (49), thus potentially connecting them functionally in LOAD. To date, 21 genes have been strongly associated with LOAD, including endocytosis genes, such as amphiphysin II (*BIN1*). An amphiphysin II-RIN3 interaction is involved in vesicle trafficking in the early endocytic pathway (21), and it is undoubtedly relevant that amphiphysin II can also bind to CD2AP (50).

Second, both RIN3 and CD2AP were among 21 proteins pulled down from kidney cells by the SH3-5/6 domains of the large adaptor protein TUBA (51). TUBA contains six SH3 domains and has guanine nucleotide exchange factor activity toward CDC42. It binds dynamin, providing a link in endocytosis to actin and actin regulatory proteins (*e.g.* Ena/VASP and N-WASP) as CD2AP binds, bundles, and caps actin (6, 15, 52). N-WASP was also present in the TUBA complex(es) along with CIN85, not surprising given its structural and functional overlap with CD2AP, as well as tight junction proteins ZO-1 and ZO-2. Interestingly, ZO-2 emerged as a hit in our peptide array screen (Fig. 3) and thus can bind to CD2AP SH3 domains directly. The proteomics study (51) did not ascertain whether or not TUBA interacted directly or was merely present in associated complexes. Therefore, a strong possibility remains that a CD2AP·RIN3 and/or a CD2AP·ZO-2 co-complex bind to TUBA, or indeed a multiprotein complex forms between several of these newly identified interacting proteins. Alongside ZO-2 and RIN3, other physiological interaction partners may feature in the array screen hits (Fig. 3), but these require further functional exploration. For instance, SYNJ2 but not SYNJ1, both of which were screen hits, was reported to interact functionally with the CD2AP homologue CIN85 (53).

Third, RIN3 was identified as a risk factor for Paget disease of bone (54), with a P386S polymorphism in RIN3e1, one of sev-

eral in the proline-rich region suggested to be functional (55). Furthermore, most recently, RIN3 has been linked to modulation of bone mineral density of the lower limbs (56). CD2AP has also been associated with the bone disorder Kashin-Beck disease (57). Thus, it is tempting to speculate that, aside from the specific environmental factors contributing to each, there may be some overlapping etiology between these diseases.

CD2AP SH3-1 was previously crystallized with peptides derived from CBL-b and CD2 (45) as heterotrimers, with two SH3-1 domains clamped around a single CBL-b or CD2 peptide. However, crystals containing CD2 heterodimers in class II orientation were also reported. The SH3-1 domain from CIN85 and β-PIX, each co-crystallized with the same CBL-b peptide, also formed heterotrimers (58). Subsequently, solution data were inconsistent with heterotrimer formation; rather, CIN85 SH3-1 most likely supported either class I or II binding in independent heterodimers (59). Most recently, a detailed biophysical study of the solution state revealed important contrasts between CIN85 and CD2AP (60). CD2AP appeared only to form heterodimers with CD2 or CBL-b peptides. Whereas a CD2 peptide bound to both CD2AP and CIN85 SH3-1 domains purely in class II orientation, CBL-b peptide could adopt class I or II arrangements with both. However, heterotrimer formation was consistent only with the CIN85 data and not CD2AP. In our study, peptides (from CBL, ALIX, and RIN3) bound with 1:1 stoichiometry, and the crystal structures confirmed heterodimers with class II orientation for both RIN3 peptides, consistent with ITC data. This is explainable by the lack of Lys or Leu in position 2 (*i.e.* $P^1(\underline{K/L})^2PxPR^6$), both of which have been proven to enable distinct partner peptides to bind in the reverse class I orientation under certain conditions (45). In addition, Arg in motif position −2, which could promote class I binding (58, 60), is absent.

The CD2AP SH3-2 structure presented herein is the first crystal structure of this domain and consequently the first high-resolution structural view of it in complex with a partner peptide; the NMR solution structure of SH3-2 alone has previously been reported (61, 62). Our crystal structure was recently used in the reconstruction of an elegant three-dimensional model of tetrameric full-length recombinant CD2AP in density maps generated by electron microscopy (EM) (63). The EM model suggests a conformational arrangement in which all SH3 domains present their binding sites accessibly. This would potentially enable SH3 interactions of individual monomers with their multiple, varied partners simultaneously, as discussed similarly in the context of CIN85 clustering (53). In short, CD2AP probably acts as a major hub in cell signaling. Consequently, how cooperativity or synergy of binding and avidity effects between the three SH3s might influence their physiological affinities and interaction dynamics is an important area of further study.

The inherent plasticity of the CD2AP SH3 domains, which is possibly a general characteristic of protein-binding modules (64), implies that there is no single, exact motif for each SH3 but rather a family of related motifs. These typically share a core of critical residues (*i.e.* P*x*(P/A)*xx*R) but diverge in the type of residue in flanking positions and their strengths of interaction. Thus, the sequence context of the binding partner dictates exactly which residues will fully determine its interaction potential. A corollary of this is the difficulty of predicting precisely which potential motif-containing proteins bind to a given SH3. On a related note, differential residue tolerances with each CD2AP SH3 were revealed by ALIX peptide permutation arrays (*e.g.* F*x*F*xx*R bound only to SH3-2 but not SH3-1 or SH3-3; Fig. 4), illustrating that selectivity can be achieved between similar SH3 domains.

Our study highlighted the usefulness of (20-aa) permutation arrays for correctly delineating all recognition determinants, because Pro in motif position 3 is interchangeable with Ala with respect to CD2AP SH3 binding. This vital information is undetectable in a simple Ala scan and hence explains why, historically, the importance of motif position 3 has often been overlooked by P → A mutagenesis studies in various experimental contexts. The permutation arrays also indicated that motifs lacking Pro or Ala in this position generally should not bind to CD2AP. This was indeed shown for the non-binding proline-rich region 1, PRR-1, in B cell linker protein, BLNK (or SLP-65), also a hit in our array screen, unlike its PRR-2 and -3, which both contain P*x*P*xx*R and were necessary and sufficient for an *in vivo* interaction (65). CIN85 has also been reported as a BLNK interactor (66).

Exactly why the SH3-1 domain bound to more partner peptides than SH3-2, such as those from CLD23, UBP51, and CSTF2, based on the same motif is not clear, given that their interactions with CBL-derived peptides exhibited a similar pattern (Fig. 2). However, the underlying reasons point toward subtle differences in physicochemical properties of the two SH3 binding surfaces governing specificity. It is noteworthy that ~34% of the screened peptides failed to bind to any CD2AP SH3 domain, although each contained a P*x*P*x*PR motif. Multiple factors may contribute to such "negative selection." For instance, *Weblogo* (67) analysis revealed a higher Gly and Pro content around the motif residues in non-binders compared with the medium/strong SH3-1 binders (Fig. 8*E*). This is rather paradoxical but implies that too little or too much rigidity could hamper adoption of the conformational state(s) optimal for binding. In line with this, the population size of preformed peptide conformers competent for binding to a partner domain surface would appear to play a decisive role in the potency of protein-peptide interactions, as demonstrated very recently for a Gab peptide interaction with Grb2 SH3-C (68). Furthermore, in the non-binding group, negatively charged side chains (Asp and Glu) are prevalent close to the critical Arg of the recognition motif but absent in binders, implying that local charge repulsion negates this positive charge required for tight binding.

The third SH3 domain is a curiosity because it bound very few of the screened peptides compared with SH3-1 and SH3-2, which displayed greater cross-similarity; its exact binding preferences are the least understood. However, SH3-3 is unique in being linked to a disease-associated mutation; a polymorphism (K301M) in SH3-3 may play a role in hereditary focal segmental glomerulosclerosis (5). Lys-301 lies outside of the canonical binding groove and so would not be expected to interfere directly with peptide ligand docking, raising questions as to its exact role. We found that SH3-3 had generally lower affinity for peptide ligands, with the exception of RIN3e2 peptide. ALIX peptide binding required a very extended sequence (Fig. 5), implicating additional contact points on the SH3 domain, yet

despite multiple attempts, we could produce no crystal structure to visualize this. An SH3-3 structure has been solved by NMR in apo form (69) and as a complex bound to ubiquitin (K_d ~130 μM) (70, 71). Ubiquitin docks partially across the P*x*(P/A)*x*pR peptide-binding groove in SH3-3 but also extends to the distal hydrophobic pocket (equivalent to that observed in the SH3-2·RIN3e2 complex); however, no prolines are present. This is probably the same site occupied by the extended ALIX motif. Subtle plasticity in the SH3 domain enabling it to accommodate aliphatic and other side chains, a general property discerned from our array data, is thus exploited in the ubiquitin interaction.

In summary, we have identified putative CD2AP SH3 binders with an *in vitro* screen using prior knowledge of recognition requirements and elucidated varied and distinct binding preferences of the three CD2AP SH3 domains with CBL, ALIX, and the novel partner RIN3. Finally, we have characterized by detailed biochemical and biophysical methods CD2AP-RIN3 interactions, revealing that RIN3 recruits CD2AP to early endosomes via two binding sites. Details of their biological interplay as well as the significance and relative importance of each SH3 domain to this and other interactions await further investigation.

Author Contributions—P. C. S. and S. M. F. designed the experiments, analyzed the results, and wrote the paper, with substantial contributions from K. H. K. and S. K. E. R., M. J., T. K., and P. C. S. performed peptide microarray and ITC experiments. P. C. S., E. R., M. J., J. R. C. M., S. K., and F. v. D. carried out protein crystallography. D. J., N. O., and R. V. designed and synthesized peptide microarrays. J. K. and K. H. K. generated DNA constructs for bacterial and mammalian cell expression and performed initial RIN cell culture and biochemistry. E. R. and M. J. purified recombinant proteins and performed mammalian cell culture and all other biochemical experiments, with P. C. S. contributing. B. R. and K. H. K. designed, performed, and analyzed the results of immunofluorescence experiments. All authors reviewed the results and approved the final version of the manuscript.

Acknowledgments—We thank members of the Structural Genomics Consortium, Oxford, for helpful interactions, in particular Tobias Krojer and also Panagis Filippakopoulos, Sarah Picaud, Georgina Berridge, Rod Chalk, and Brian Marsden; Moin A. Saleem (University of Bristol) for provision of kidney podocytes and advice on culture techniques; and Toshiaki Katada for the RFP- and Myc-tagged RIN3 constructs.

References

1. Dustin, M. L., Olszowy, M. W., Holdorf, A. D., Li, J., Bromley, S., Desai, N., Widder, P., Rosenberger, F., van der Merwe, P. A., Allen, P. M., and Shaw, A. S. (1998) A novel adaptor protein orchestrates receptor patterning and cytoskeletal polarity in T-cell contacts. *Cell* **94,** 667–677
2. Kirsch, K. H., Georgescu, M. M., Ishimaru, S., and Hanafusa, H. (1999) CMS: an adapter molecule involved in cytoskeletal rearrangements. *Proc. Natl. Acad. Sci. U.S.A.* **96,** 6211–6216
3. Shih, N.-Y., Li, J., Karpitskii, V., Nguyen, A., Dustin, M. L., Kanagawa, O., Miner, J. H., and Shaw, A. S. (1999) Congenital nephrotic syndrome in mice lacking CD2-associated protein. *Science* **286,** 312–315
4. Löwik, M. M., Groenen, P. J., Pronk, I., Lilien, M. R., Goldschmeding, R., Dijkman, H. B., Levtchenko, E. N., Monnens, L. A., and van den Heuvel, L. P. (2007) Focal segmental glomerulosclerosis in a patient homozygous for a CD2AP mutation. *Kidney Int.* **72,** 1198–1203
5. Gigante, M., Pontrelli, P., Montemurno, E., Roca, L., Aucella, F., Penza, R., Caridi, G., Ranieri, E., Ghiggeri, G. M., and Gesualdo, L. (2009) CD2AP mutations are associated with sporadic nephrotic syndrome and focal segmental glomerulosclerosis (FSGS). *Nephrol. Dial. Transplant.* **24,** 1858–1864
6. Gaidos, G., Soni, S., Oswald, D. J., Toselli, P. A., and Kirsch, K. H. (2007) Structure and function analysis of the CMS/CIN85 protein family identifies actin-bundling properties and heterotypic-complex formation. *J. Cell Sci.* **120,** 2366–2377
7. Lynch, D. K., Winata, S. C., Lyons, R. J., Hughes, W. E., Lehrbach, G. M., Wasinger, V., Corthals, G., Cordwell, S., and Daly, R. J. (2003) A Cortactin-CD2-associated protein (CD2AP) complex provides a novel link between epidermal growth factor receptor endocytosis and the actin cytoskeleton. *J. Biol. Chem.* **278,** 21805–21813
8. Kobayashi, S., Sawano, A., Nojima, Y., Shibuya, M., and Maru, Y. (2004) The c-Cbl/CD2AP complex regulates VEGF-induced endocytosis and degradation of Flt-1 (VEGFR-1). *FASEB J.* **18,** 929–931
9. Lee, K. H., Dinner, A. R., Tu, C., Campi, G., Raychaudhuri, S., Varma, R., Sims, T. N., Burack, W. R., Wu, H., Wang, J., Kanagawa, O., Markiewicz, M., Allen, P. M., Dustin, M. L., Chakraborty, A. K., and Shaw, A. S. (2003) The immunological synapse balances T cell receptor signaling and degradation. *Science* **302,** 1218–1222
10. Minegishi, Y., Shibagaki, Y., Mizutani, A., Fujita, K., Tezuka, T., Kinoshita, M., Kuroda, M., Hattori, S., and Gotoh, N. (2013) Adaptor protein complex of FRS2β and CIN85/CD2AP provides a novel mechanism for ErbB2/HER2 protein downregulation. *Cancer Sci.* **104,** 345–352
11. Tsui, C. C., and Pierchala, B. A. (2008) CD2AP and Cbl-3/Cbl-c constitute a critical checkpoint in the regulation of ret signal transduction. *J. Neurosci.* **28,** 8789–8800
12. Calco, G. N., Stephens, O. R., Donahue, L. M., Tsui, C. C., and Pierchala, B. A. (2014) CD2-associated protein (CD2AP) enhances casitas B lineage lymphoma-3/c (Cbl-3/c)-mediated Ret isoform-specific ubiquitination and degradation via its amino-terminal Src homology 3 domains. *J. Biol. Chem.* **289,** 7307–7319
13. Bao, M., Hanabuchi, S., Facchinetti, V., Du, Q., Bover, L., Plumas, J., Chaperot, L., Cao, W., Qin, J., Sun, S. C., and Liu, Y. J. (2012) CD2AP/SHIP1 complex positively regulates plasmacytoid dendritic cell receptor signaling by inhibiting the E3 ubiquitin ligase Cbl. *J. Immunol.* **189,** 786–792
14. Zhao, J., Bruck, S., Cemerski, S., Zhang, L., Butler, B., Dani, A., Cooper, J. A., and Shaw, A. S. (2013) CD2AP links cortactin and capping protein at the cell periphery to facilitate formation of lamellipodia. *Mol. Cell Biol.* **33,** 38–47
15. Tang, V. W., and Brieher, W. M. (2013) FSGS3/CD2AP is a barbed-end capping protein that stabilizes actin and strengthens adherens junctions. *J. Cell Biol.* **203,** 815–833
16. Kirsch, K. H., Georgescu, M. M., Shishido, T., Langdon, W. Y., Birge, R. B., and Hanafusa, H. (2001) The adapter type protein CMS/CD2AP binds to the proto-oncogenic protein c-Cbl through a tyrosine phosphorylation-regulated Src homology 3 domain interaction. *J. Biol. Chem.* **276,** 4957–4963
17. Haglund, K., Shimokawa, N., Szymkiewicz, I., and Dikic, I. (2002) Cbl-directed monoubiquitination of CIN85 is involved in regulation of ligand-induced degradation of EGF receptors. *Proc. Natl. Acad. Sci. U.S.A.* **99,** 12191–12196
18. Tan, M. S., Yu, J. T., and Tan, L. (2013) Bridging integrator 1 (BIN1): form, function, and Alzheimer's disease. *Trends Mol. Med.* **19,** 594–603
19. Hollingworth, P., Harold, D., Sims, R., Gerrish, A., Lambert, J.-C., Carrasquillo, M. M., Abraham, R., Hamshere, M. L., Pahwa, J. S., Moskvina, V., Dowzell, K., Jones, N., Stretton, A., Thomas, C., Richards, A., Ivanov, D., Widdowson, C., Chapman, J., Lovestone, S., Powell, J., Proitsi, P., Lupton, M. K., Brayne, C., Rubinsztein, D. C., Gill, M., Lawlor, B., Lynch, A., Brown, K. S., Passmore, P. A., Craig, D., McGuinness, B., Todd, S., Holmes, C., Mann, D., Smith, A. D., Beaumont, H., Warden, D., Wilcock, G., Love, S., Kehoe, P. G., Hooper, N. M., Vardy, E. R., Hardy, J., Mead, S., Fox, N. C., Rossor, M., Collinge, J., Maier, W., Jessen, F., Rüther, E., Schürmann, B., *et al.* (2011) Common variants at ABCA7, MS4A6A/MS4A4E, EPHA1, CD33 and CD2AP are associated with Alzheimer's disease. *Nat. Genet.* **43,** 429–435
20. Naj, A. C., Jun, G., Beecham, G. W., Wang, L. S., Vardarajan, B. N., Buros,

J., Gallins, P. J., Buxbaum, J. D., Jarvik, G. P., Crane, P. K., Larson, E. B., Bird, T. D., Boeve, B. F., Graff-Radford, N. R., De Jager, P. L., Evans, D., Schneider, J. A., Carrasquillo, M. M., Ertekin-Taner, N., Younkin, S. G., Cruchaga, C., Kauwe, J. S., Nowotny, P., Kramer, P., Hardy, J., Huentelman, M. J., Myers, A. J., Barmada, M. M., Demirci, F. Y., Baldwin, C. T., Green, R. C., Rogaeva, E., St George-Hyslop, P., Arnold, S. E., Barber, R., Beach, T., Bigio, E. H., Bowen, J. D., Boxer, A., Burke, J. R., Cairns, N. J., Carlson, C. S., Carney, R. M., Carroll, S. L., Chui, H. C., Clark, D. G., Corneveaux, J., Cotman, C. W., Cummings, J. L., DeCarli, C., DeKosky, S. T., *et al.* (2011) Common variants at MS4A4/MS4A6E, CD2AP, CD33 and EPHA1 are associated with late-onset Alzheimer's disease. *Nat. Genet.* **43,** 436–441

21. Kajiho, H., Saito, K., Tsujita, K., Kontani, K., Araki, Y., Kurosu, H., and Katada, T. (2003) RIN3: a novel Rab5 GEF interacting with amphiphysin II involved in the early endocytic pathway. *J. Cell Sci.* **116,** 4159–4168
22. Kajiho, H., Sakurai, K., Minoda, T., Yoshikawa, M., Nakagawa, S., Fukushima, S., Kontani, K., and Katada, T. (2011) Characterization of RIN3 as a guanine nucleotide exchange factor for the Rab5 subfamily GTPase Rab31. *J. Biol. Chem.* **286,** 24364–24373
23. Kirsch, K. H., Georgescu, M. M., and Hanafusa, H. (1998) Direct binding of p130(Cas) to the guanine nucleotide exchange factor C3G. *J. Biol. Chem.* **273,** 25673–25679
24. Saito, K., Murai, J., Kajiho, H., Kontani, K., Kurosu, H., and Katada, T. (2002) A novel binding protein composed of homophilic tetramer exhibits unique properties for the small GTPase Rab5. *J. Biol. Chem.* **277,** 3412–3418
25. Harkiolaki, M., Tsirka, T., Lewitzky, M., Simister, P. C., Joshi, D., Bird, L. E., Jones, E. Y., O'Reilly, N., and Feller, S. M. (2009) Distinct binding modes of two epitopes in Gab2 that interact with the SH3C domain of Grb2. *Structure* **17,** 809–822
26. Landgraf, C., Panni, S., Montecchi-Palazzi, L., Castagnoli, L., Schneider-Mergener, J., Volkmer-Engert, R., and Cesareni, G. (2004) Protein interaction networks by proteome peptide scanning. *PLoS Biol.* **2,** E14
27. Tonikian, R., Xin, X., Toret, C. P., Gfeller, D., Landgraf, C., Panni, S., Paoluzi, S., Castagnoli, L., Currell, B., Seshagiri, S., Yu, H., Winsor, B., Vidal, M., Gerstein, M. B., Bader, G. D., Volkmer, R., Cesareni, G., Drubin, D. G., Kim, P. M., Sidhu, S. S., and Boone, C. (2009) Bayesian modeling of the yeast SH3 domain interactome predicts spatiotemporal dynamics of endocytosis proteins. *PLoS Biol.* **7,** e1000218
28. Simister, P. C., Schaper, F., O'Reilly, N., McGowan, S., and Feller, S. M. (2011) Self-organization and regulation of intrinsically disordered proteins with folded N-termini. *PLoS Biol.* **9,** e1000591
29. de Castro, E., Sigrist, C. J. A., Gattiker, A., Bulliard, V., Langendijk-Genevaux, P. S., Gasteiger, E., Bairoch, A., and Hulo, N. (2006) ScanProsite: detection of PROSITE signature matches and ProRule-associated functional and structural residues in proteins. *Nucleic Acids Res.* **34,** W362–W365
30. Simister, P. C., Luccarelli, J., Thompson, S., Appella, D. H., Feller, S. M., and Hamilton, A. D. (2013) Novel inhibitors of a Grb2 SH3C domain interaction identified by a virtual screen. *Bioorg. Med. Chem.* **21,** 4027–4033
31. Kabsch, W. (2010) XDS. *Acta Crystallogr. D Biol. Crystallogr.* **66,** 125–132
32. Evans, P. (2006) Scaling and assessment of data quality. *Acta Crystallogr. D Biol. Crystallogr.* **62,** 72–82
33. McCoy, A. J., Grosse-Kunstleve, R. W., Adams, P. D., Winn, M. D., Storoni, L. C., and Read, R. J. (2007) *Phaser* crystallographic software. *J. Appl. Crystallogr.* **40,** 658–674
34. Murshudov, G. N., Vagin, A. A., and Dodson, E. J. (1997) Refinement of macromolecular structures by the maximum-likelihood method. *Acta Crystallogr. D* **53,** 240–255
35. Emsley, P., Lohkamp, B., Scott, W. G., and Cowtan, K. (2010) Features and development of Coot. *Acta Crystallogr. D Biol. Crystallogr.* **66,** 486–501
36. Adams, P. D., Afonine, P. V., Bunkóczi, G., Chen, V. B., Davis, I. W., Echols, N., Headd, J. J., Hung, L.-W., Kapral, G. J., Grosse-Kunstleve, R. W., McCoy, A. J., Moriarty, N. W., Oeffner, R., Read, R. J., Richardson, D. C., Richardson, J. S., Terwilliger, T. C., and Zwart, P. H. (2010) PHENIX: a comprehensive Python-based system for macromolecular structure solution. *Acta Crystallogr. D Biol. Crystallogr.* **66,** 213–221
37. Ni, L., Saleem, M., and Mathieson, P. W. (2012) Podocyte culture: tricks of the trade. *Nephrology* **17,** 525–531
38. Debnath, J., Muthuswamy, S. K., and Brugge, J. S. (2003) Morphogenesis and oncogenesis of MCF-10A mammary epithelial acini grown in three-dimensional basement membrane cultures. *Methods* **30,** 256–268
39. Kumbrink, J., and Kirsch, K. H. (2012) Regulation of p130(Cas)/BCAR1 expression in tamoxifen-sensitive and tamoxifen-resistant breast cancer cells by EGR1 and NAB2. *Neoplasia* **14,** 108–120
40. Emaduddin, M., Bicknell, D. C., Bodmer, W. F., and Feller, S. M. (2008) Cell growth, global phosphotyrosine elevation, and c-Met phosphorylation through Src family kinases in colorectal cancer cells. *Proc. Natl. Acad. Sci. U.S.A.* **105,** 2358–2362
41. Janson, C., Kasahara, N., Prendergast, G. C., and Colicelli, J. (2012) RIN3 is a negative regulator of mast cell responses to SCF. *PLoS One* **7,** e49615
42. Kowanetz, K., Szymkiewicz, I., Haglund, K., Kowanetz, M., Husnjak, K., Taylor, J. D., Soubeyran, P., Engstrom, U., Ladbury, J. E., and Dikic, I. (2003) Identification of a novel proline-arginine motif involved in CIN85-dependent clustering of Cbl and down-regulation of epidermal growth factor receptors. *J. Biol. Chem.* **278,** 39735–39746
43. Huang, F., and Sorkin, A. (2005) Growth factor receptor binding protein 2-mediated recruitment of the RING domain of Cbl to the epidermal growth factor receptor is essential and sufficient to support receptor endocytosis. *Mol. Biol. Cell* **16,** 1268–1281
44. Buday, L., Khwaja, A., Sipeki, S., Faragó, A., and Downward, J. (1996) Interactions of Cbl with two adapter proteins, Grb2 and Crk, upon T cell activation. *J. Biol. Chem.* **271,** 6159–6163
45. Moncalián, G., Cárdenes, N., Deribe, Y. L., Spínola-Amilibia, M., Dikic, I., and Bravo, J. (2006) Atypical polyproline recognition by the CMS N-terminal Src homology 3 domain. *J. Biol. Chem.* **281,** 38845–38853
46. Filippakopoulos, P., Picaud, S., Mangos, M., Keates, T., Lambert, J. P., Barsyte-Lovejoy, D., Felletar, I., Volkmer, R., Müller, S., Pawson, T., Gingras, A. C., Arrowsmith, C. H., and Knapp, S. (2012) Histone recognition and large-scale structural analysis of the human bromodomain family. *Cell* **149,** 214–231
47. Usami, Y., Popov, S., and Göttlinger, H. G. (2007) Potent rescue of human immunodeficiency virus type 1 late domain mutants by ALIX/AIP1 depends on its CHMP4 binding site. *J. Virol.* **81,** 6614–6622
48. Philippe, D., Ababou, A., Yang, X., Ghosh, R., Daviter, T., Ladbury, J. E., and Pfuhl, M. (2011) Making ends meet: the importance of the N- and C-termini for the structure, stability, and function of the third SH3 domain of CIN85. *Biochemistry* **50,** 3649–3659
49. Lambert, J. C., Ibrahim-Verbaas, C. A., Harold, D., Naj, A. C., Sims, R., Bellenguez, C., DeStafano, A. L., Bis, J. C., Beecham, G. W., Grenier-Boley, B., Russo, G., Thorton-Wells, T. A., Jones, N., Smith, A. V., Chouraki, V., Thomas, C., Ikram, M. A., Zelenika, D., Vardarajan, B. N., Kamatani, Y., Lin, C. F., Gerrish, A., Schmidt, H., Kunkle, B., Dunstan, M. L., Ruiz, A., Bihoreau, M. T., Choi, S. H., Reitz, C., Pasquier, F., Cruchaga, C., Craig, D., Amin, N., Berr, C., Lopez, O. L., De Jager, P. L., Deramecourt, V., Johnston, J. A., Evans, D., Lovestone, S., Letenneur, L., Morón, F. J., Rubinsztein, D. C., Eiriksdottir, G., Sleegers, K., Goate, A. M., Fiévet, N., Huentelman, M. W., Gill, M., Brown, K., Kamboh, M. I., *et al.* (2013) Meta-analysis of 74,046 individuals identifies 11 new susceptibility loci for Alzheimer's disease. *Nat. Genet.* **45,** 1452–1458
50. Neuvonen, M., Kazlauskas, A., Martikainen, M., Hinkkanen, A., Ahola, T., and Saksela, K. (2011) SH3 domain-mediated recruitment of host cell amphiphysins by alphavirus nsP3 promotes viral RNA replication. *PLoS Pathog.* **7,** e1002383
51. Jin, J., Xie, X., Chen, C., Park, J. G., Stark, C., James, D. A., Olhovsky, M., Linding, R., Mao, Y., and Pawson, T. (2009) Eukaryotic protein domains as functional units of cellular evolution. *Sci. Signal.* **2,** ra76
52. Lehtonen, S., Zhao, F., and Lehtonen, E. (2002) CD2-associated protein directly interacts with the actin cytoskeleton. *Am. J. Physiol. Renal Physiol.* **283,** F734–F743
53. Kowanetz, K., Husnjak, K., Höller, D., Kowanetz, M., Soubeyran, P., Hirsch, D., Schmidt, M. H. H., Pavelic, K., De Camilli, P., Randazzo, P. A., and Dikic, I. (2004) CIN85 associates with multiple effectors controlling intracellular trafficking of epidermal growth factor receptors. *Mol. Biol. Cell* **15,** 3155–3166
54. Albagha, O. M., Wani, S. E., Visconti, M. R., Alonso, N., Goodman, K.,

Brandi, M. L., Cundy, T., Chung, P. Y., Dargie, R., Devogelaer, J. P., Falchetti, A., Fraser, W. D., Gennari, L., Gianfrancesco, F., Hooper, M. J., Van Hul, W., Isaia, G., Nicholson, G. C., Nuti, R., Papapoulos, S., Montes Jdel, P., Ratajczak, T., Rea, S. L., Rendina, D., Gonzalez-Sarmiento, R., Di Stefano, M., Ward, L. C., Walsh, J. P., Ralston, S. H., and Genetic Determinants of Paget's Disease (GDPD) Consortium (2011) Genome-wide association identifies three new susceptibility loci for Paget's disease of bone. *Nat. Genet.* **43,** 685–689

55. Vallet, M., Soares, D. C., Wani, S., Sophocleous, A., Warner, J., Salter, D. M., Ralston, S. H., Albagha, O. M. (2015) Targeted sequencing of the Paget's disease associated 14q32 locus identifies several missense coding variants in RIN3 that predispose to Paget's disease of bone. *Hum. Mol. Genet.* **24,** 3286–3295
56. Kemp, J. P., Medina-Gomez, C., Estrada, K., St Pourcain, B., Heppe, D. H., Warrington, N. M., Oei, L., Ring, S. M., Kruithof, C. J., Timpson, N. J., Wolber, L. E., Reppe, S., Gautvik, K., Grundberg, E., Ge, B., van der Eerden, B., van de Peppel, J., Hibbs, M. A., Ackert-Bicknell, C. L., Choi, K., Koller, D. L., Econs, M. J., Williams, F. M., Foroud, T., Zillikens, M. C., Ohlsson, C., Hofman, A., Uitterlinden, A. G., Davey Smith, G., Jaddoe, V. W., Tobias, J. H., Rivadeneira, F., and Evans, D. M. (2014) Phenotypic dissection of bone mineral density reveals skeletal site specificity and facilitates the identification of novel loci in the genetic regulation of bone mass attainment. *PLoS Genet.* **10,** e1004423
57. Yang, Z., Xu, Y., Luo, H., Ma, X., Wang, Q., Wang, Y., Deng, W., Jiang, T., Sun, G., He, T., Hu, J., Li, Y., Wang, J., Li, T., and Hu, X. (2014) Whole-exome sequencing for the identification of susceptibility genes of Kashin-Beck disease. *PLoS One* **9,** e92298
58. Jozic, D., Cárdenes, N., Deribe, Y. L., Moncalián, G., Hoeller, D., Groemping, Y., Dikic, I., Rittinger, K., and Bravo, J. (2005) Cbl promotes clustering of endocytic adaptor proteins. *Nat. Struct. Mol. Biol.* **12,** 972–979
59. Ababou, A., Pfuhl, M., and Ladbury, J. E. (2009) Novel insights into the mechanisms of CIN85 SH3 domains binding to Cbl proteins: solution-based investigations and *in vivo* implications. *J. Mol. Biol.* **387,** 1120–1136
60. Ceregido, M. A., Garcia-Pino, A., Ortega-Roldan, J. L., Casares, S., López Mayorga, O., Bravo, J., van Nuland, N. A., and Azuaga, A. I. (2013) Multimeric and differential binding of CIN85/CD2AP with two atypical proline-rich sequences from CD2 and Cbl-b. *FEBS J.* **280,** 3399–3415
61. Yao, B., Zhang, J., Dai, H., Sun, J., Jiao, Y., Tang, Y., Wu, J., and Shi, Y. (2007) Solution structure of the second SH3 domain of human CMS and a newly identified binding site at the C-terminus of c-Cbl. *Biochim. Biophys. Acta* **1774,** 35–43
62. Ortega-Roldan, J. L., Blackledge, M., van Nuland, N. A. J., and Azuaga, A. I. (2011) Solution structure, dynamics and thermodynamics of the three SH3 domains of CD2AP. *J. Biomol. NMR* **50,** 103–117
63. Adair, B. D., Altintas, M. M., Möller, C. C., Arnaout, M. A., and Reiser, J. (2014) Structure of the kidney slit diaphragm adapter protein CD2-associated protein as determined with electron microscopy. *J. Am. Soc. Nephrol.* **25,** 1465–1473
64. Stollar, E. J., Lin, H., Davidson, A. R., and Forman-Kay, J. D. (2012) Differential dynamic engagement within 24 SH3 domain:peptide complexes revealed by co-linear chemical shift perturbation analysis. *PLoS One* **7,** e51282
65. Oellerich, T., Bremes, V., Neumann, K., Bohnenberger, H., Dittmann, K., Hsiao, H. H., Engelke, M., Schnyder, T., Batista, F. D., Urlaub, H., and Wienands, J. (2011) The B-cell antigen receptor signals through a preformed transducer module of SLP65 and CIN85. *EMBO J.* **30,** 3620–3634
66. Watanabe, S., Take, H., Takeda, K., Yu, Z. X., Iwata, N., and Kajigaya, S. (2000) Characterization of the CIN85 adaptor protein and identification of components involved in CIN85 complexes. *Biochem. Biophys. Res. Commun.* **278,** 167–174
67. Crooks, G. E., Hon, G., Chandonia, J. M., and Brenner, S. E. (2004) WebLogo: a sequence logo generator. *Genome Res.* **14,** 1188–1190
68. Krieger, J. M., Fusco, G., Lewitzky, M., Simister, P. C., Marchant, J., Camilloni, C., Feller, S. M., and De Simone, A. (2014) Conformational recognition of an intrinsically disordered protein. *Biophys. J.* **106,** 1771–1779
69. Ortega Roldan, J. L., Romero Romero, M. L., Ora, A., Ab, E., Lopez Mayorga, O., Azuaga, A. I., and van Nuland, N. A. (2007) The high resolution NMR structure of the third SH3 domain of CD2AP. *J. Biomol. NMR* **39,** 331–336
70. Ortega-Roldan, J. L., Jensen, M. R., Brutscher, B., Azuaga, A. I., Blackledge, M., and van Nuland, N. A. (2009) Accurate characterization of weak macromolecular interactions by titration of NMR residual dipolar couplings: application to the CD2AP SH3-C:ubiquitin complex. *Nucleic Acids Res.* **37,** e70
71. Ortega Roldan, J. L., Casares, S., Ringkjøbing Jensen, M., Cárdenes, N., Bravo, J., Blackledge, M., Azuaga, A. I., and van Nuland, N. A. (2013) Distinct ubiquitin binding modes exhibited by SH3 domains: molecular determinants and functional implications. *PLoS One* **8,** e73018